

APPENDIX III: DESCRIPTION OF THE SUBROUTINES

Contents

Description of the file used to control the accuracy of RT simulations

FILE PARAMDEF.INC 60

Description of the subroutines used to compute the geometrical conditions:

SUBROUTINE POSGE 62

SUBROUTINE POSGW 63

SUBROUTINE POSLAN 64

SUBROUTINE POSMTO 65

SUBROUTINE POSNOA 71

SUBROUTINE POSSOL 75

SUBROUTINE POSSPO 79

Description of the subroutines used to compute the atmospheric conditions:

SUBROUTINE ABSTRA 81

SUBROUTINE AEROSO 87

SUBROUTINE AEROPROF 93

SUBROUTINE ATMREF 94

SUBROUTINE CSALBR 96

SUBROUTINE DISCOM 97

SUBROUTINE DISCRE 98

SUBROUTINE ENVIRO 99

SUBROUTINE GAUSS 104

SUBROUTINE INTERP 105

SUBROUTINE ISO 106

SUBROUTINE KERNEL (and KERNELPOL) 107

SUBROUTINE MIE (and EXSCPHASE) 108

SUBROUTINE ODA550 128

SUBROUTINE ODRAYL 130

SUBROUTINE OSPOL	132
SUBROUTINE SCATRA	135
SUBROUTINE TRUNCA	137

Description of the subroutines used to compute ground BRDF:

SUBROUTINE HAPKALBE	139
SUBROUTINE IAPIALBE	140
SUBROUTINE MINNALBE	140
SUBROUTINE OCEALBE (and GLITALBE)	140
SUBROUTINE RAHMALBE	140
SUBROUTINE ROUJALBE	140
SUBROUTINE VERSALBE	140
SUBROUTINE WALTALBE	140
SUBROUTINE BRDFGRID	141
SUBROUTINE HAPKBRDF	142
SUBROUTINE IAPIBRDF	144
SUBROUTINE MINNBRDF	147
SUBROUTINE OCEABRDF (and OCEATOOLS)	148
SUBROUTINE RAHMBRDF	158
SUBROUTINE ROUJBRDF	160
SUBROUTINE VERSBRDF	162
SUBROUTINE WALTBRDF	166
SUBROUTINE AKBRDF	167
SUBROUTINE AKLABE	171
SUBROUTINE MODISBRDF	172
SUBROUTINE MODISALBE	174

Description of the subroutines used to update the atmospheric profile (airplane or elevated target simulations):

SUBROUTINE PRESPLANE	176
SUBROUTINE PRESSURE	177

Description of the subroutines used to read the data:

SUBROUTINE SOLIRR	179
SUBROUTINE VARSOL	180
SUBROUTINE AATSR	181
SUBROUTINE ALI	183
SUBROUTINE ASTER	185
SUBROUTINE AVHRR	187
SUBROUTINE ETM	191
SUBROUTINE GLI	193
SUBROUTINE GOES	199
SUBROUTINE HRV	200
SUBROUTINE HYPBLUE	202
SUBROUTINE MAS	203
SUBROUTINE MERIS	205
SUBROUTINE METEO	208
SUBROUTINE MODIS	209
SUBROUTINE MSS	211
SUBROUTINE POLDER	212
SUBROUTINE SEAWIFS	214
SUBROUTINE TM	216
SUBROUTINE VGT	218
SUBROUTINE VIIRS	219
SUBROUTINE CLEARW	222
SUBROUTINE LAKEW	223
SUBROUTINE SAND	224
SUBROUTINE VEGETA	225
SUBROUTINE DICA 1 TO 3	226
SUBROUTINE METH 1 TO 6	227
SUBROUTINE MOCA 1 TO 6	228
SUBROUTINE NIOX 1 TO 6	229
SUBROUTINE OXYG 3 TO 6	230

SUBROUTINE OZON 1	231
SUBROUTINE WAVA 1 TO 6	233
SUBROUTINE DUST	233
SUBROUTINE OCEA	233
SUBROUTINE SOOT	233
SUBROUTINE WATE	233
SUBROUTINE BBM	234
SUBROUTINE BDM	234
SUBROUTINE STM	234
SUBROUTINE MIDSUM	235
SUBROUTINE MIDWIN	236
SUBROUTINE SUBSUM	238
SUBROUTINE SUBWIN	238
SUBROUTINE TROPIC	239
SUBROUTINE US62	240
Miscellaneous:	
SUBROUTINE EQUIVWL	242
SUBROUTINE PRINT_ERROR	243
SUBROUTINE SPECINTERP	244
SUBROUTINE SPLIE2, SPLIN2, SPLINE, & SPLINT	245

FILE PARAMDEF.INC

Function: To control the accuracy of 6SV calculations.

Description: This file gives the experienced user the possibility to control the accuracy of RT simulations by changing the number of calculation layers (nt_p), zenith calculation angles (mu_p), azimuth calculation angles (nfi_p), and Legendre coefficients (nquad_p, for aerosol calculations). By default, these parameters are fixed to the following values: nt_p = 30, mu_p = 25, nfi_p = 181, and nquad_p = 83, which in general provides a good accuracy of 0.4-0.6%, compared to other RT codes and benchmarks.

DESCRIPTION OF THE SUBROUTINES USED

TO COMPUTE THE GEOMETRICAL CONDITIONS

SUBROUTINE POSGE

Function: Same as POSMTO but for the GOES East satellite. We use exactly the same scheme but added the longitude of the sub-satellite point, namely 75°W , at the retrieval longitude. Let us also recall that the dimension of the frame is 17331×12997 and the altitude of the satellite is 35729 km.

SUBROUTINE POSGW

Function: Same as POSMTO but for the GOES West satellite. We use exactly the same scheme but added the longitude of the sub-satellite point, namely 135°W, at the retrieval longitude. Let us recall that the dimension of the frame is 17331×12997 and the altitude of the satellite is 35769 km.

SUBROUTINE POSLAN

Function: To compute the geometrical conditions for the LANDSAT satellite. As the dimensions of the frame are 180×180 km, the maximum observation angle is 5.5° , so we put $\theta_v=0$. The incident conditions are taken from the latitude and longitude of the centre of the scene.

Reference:

NASA GSFC specification for the thematic mapper subsystem and associated test equipment. revision C, GSFC 400-8-D.210C, NASA/GSFC, Greenbelt, Maryland, USA, 1981.

SUBROUTINE POSMTO

Function: To compute geometrical conditions from the knowledge of the line number and pixel in the line (in the Meteosat Frame 2500*5000). First, we compute the latitude and longitude of a given pixel to define the solar position (with the time conditions). Second, we compute the observation angle.

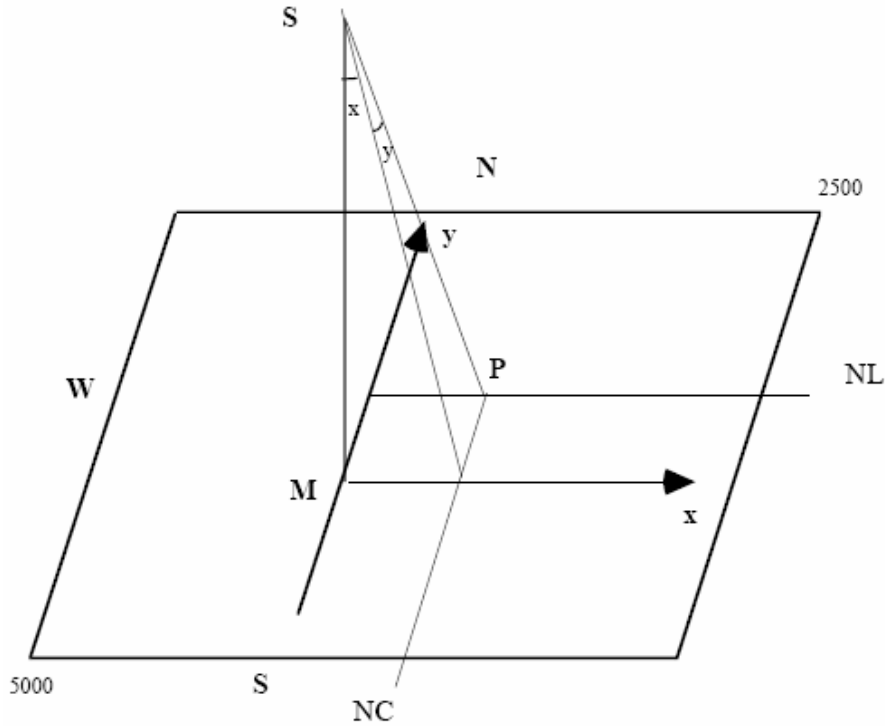


Fig. 1.

Description: Let S be the satellite, M the subsatellite point, P the observed point, and the orientation of the axes according to Fig. 1. From N_c and N_l , we obtain the two angles X and Y with respect to the x and y axes. If we now refer to the plane containing the points S, P, M and the center of the earth O (see Fig. 2), we put the altitude of the satellite H and the earth radius R_E in the equatorial plane. The observed point P corresponds to the point P' on the earth surface and we have to determine its coordinates x, y, z with respect to the axis-system centered at O.

where

$$\cos^2 X = \frac{1}{1 + \tan^2 X}$$

and

$$\cos^2 Y = \frac{1}{1 + (\tan Y(1 + \varepsilon))^2}$$

with

$$\varepsilon = \frac{R_E - R_P}{R_E} = \frac{1}{297}$$

Here R_E and R_P are the equatorial and polar radii, which are slightly different because of the Earth's oblateness.

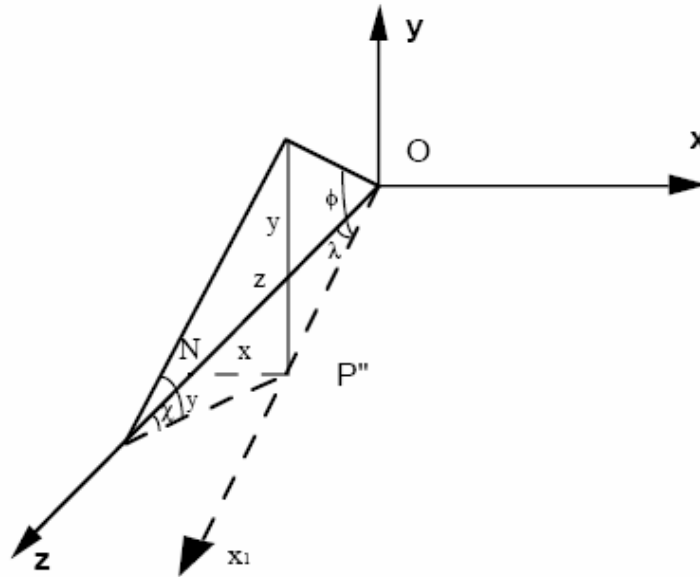


Fig. 3.

To obtain x and y , we consider the Fig. 3:

$$x = -SN \tan Y \text{ and } y = SN / \cos X \cdot \tan Y.$$

So, we have the three coordinates x , y , and z of the point P' and infer latitude ϕ and longitude λ . To compute the longitude, we use $\lambda = \arctan(x/z)$ (+ for East, - for West). To compute the latitude, we have to consider the geoid with the semiminor axis R_P and semimajor axis R_E (Fig. 4) by solving triangle $P'OP''$. As $\phi = \arctan(y/x_1)$ where y is the ordinate of the point located on the ellipsoid, we have to compute x_1 .

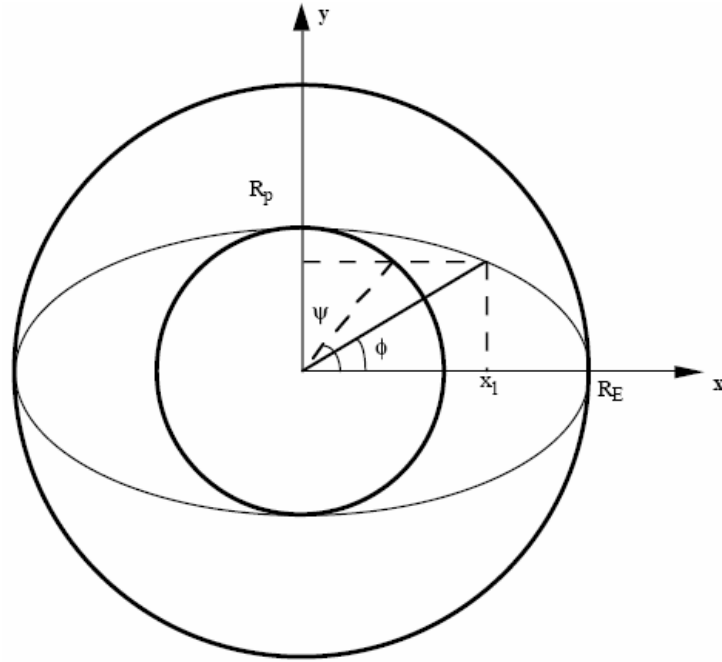


Fig. 4.

The ellipse equation is written:

$$\frac{x_1^2}{R_E^2} + \frac{y^2}{R_p^2} = 1$$

so

$$\phi = a \tan \left(\frac{y}{\sqrt{R_p^2 - y^2 (R_p / R_E)}} \right),$$

$$\phi = a \tan(\tan \Psi (R_p / R_E))$$

with $\Psi = a \sin(y / R_p)$

To obtain observation angles (azimuth and zenith), we use the following simple geometrical considerations. For the zenith angle θ_v ,

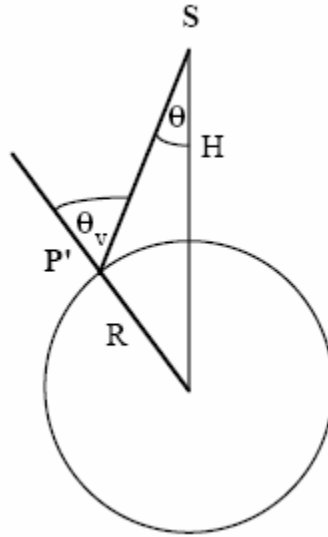


Fig. 5.

$$\theta_v = a \sin \left(\left(1 + \frac{H}{R} \right) \sin \theta \right),$$

where θ is so that $\cos^2 \theta_v = \cos^2 X \cos^2 Y$.

For the azimuthal angle ϕ_v , we solve the spherical triangle P'P''M

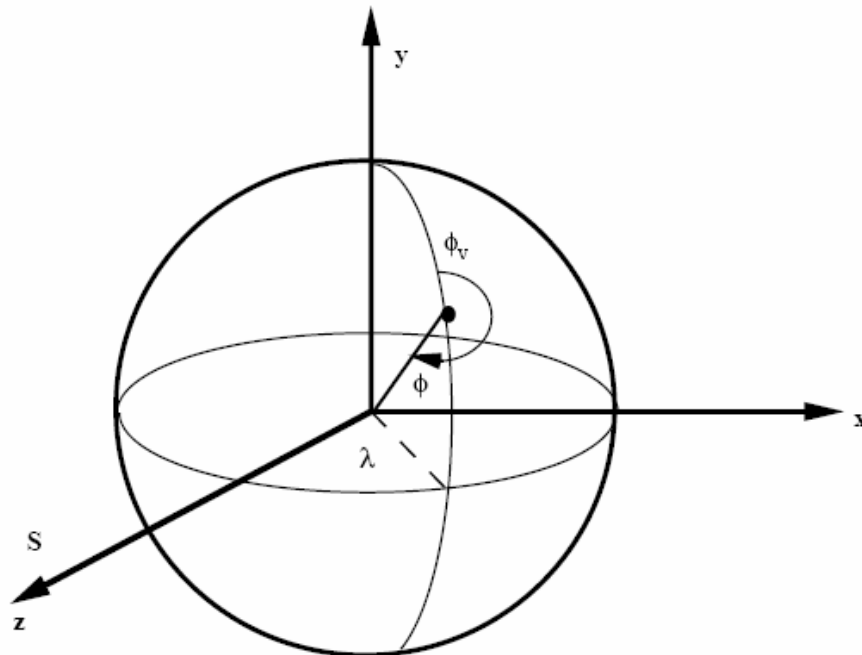


Fig. 6.

where $A = \phi_v - \pi$,

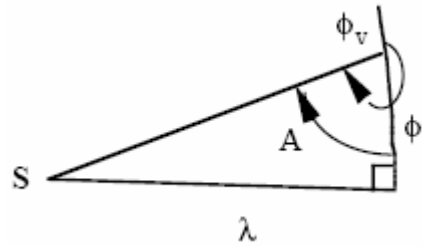


Fig. 7.

with $\tan A = \tan \lambda (1 / \sin \phi)$,

so $\phi_v = \arctan[\tan \lambda (1 / \sin \phi)] + \pi$.

From the line and column numbers in the METEOSAT frame, we can compute the latitude (ϕ) and longitude (λ) of the point, and viewing direction from the normal at the point (azimuth ϕ_v and zenith θ_v angles). Moreover, if we know the date and hour of the acquisition, we can obtain the solar conditions (θ_s, ϕ_s) from the subroutine POSSOL.

Reference:

J. Morgan, Introduction to the Meteosat system, ESOC, Darmstadt, Germany, 1981.

SUBROUTINE POSNOA

Function: To compute the geometrical conditions for the NOAA series satellites. Generally, we know the pixel number on a line, longitude and time of the ascendant node at the equator, and time of acquisition. We obtain the latitude and longitude of the viewed point, viewing angles and, with the knowledge of the date, solar geometrical conditions.

Description: The altitude of the NOAA satellite is about $H = 860$ km, orbit inclination is 98.96° and time of one revolution is about 101.98 min (6119 sec.). The $1/2$ angle is of maximum 55.385° and there are 2048 pixels for each line.

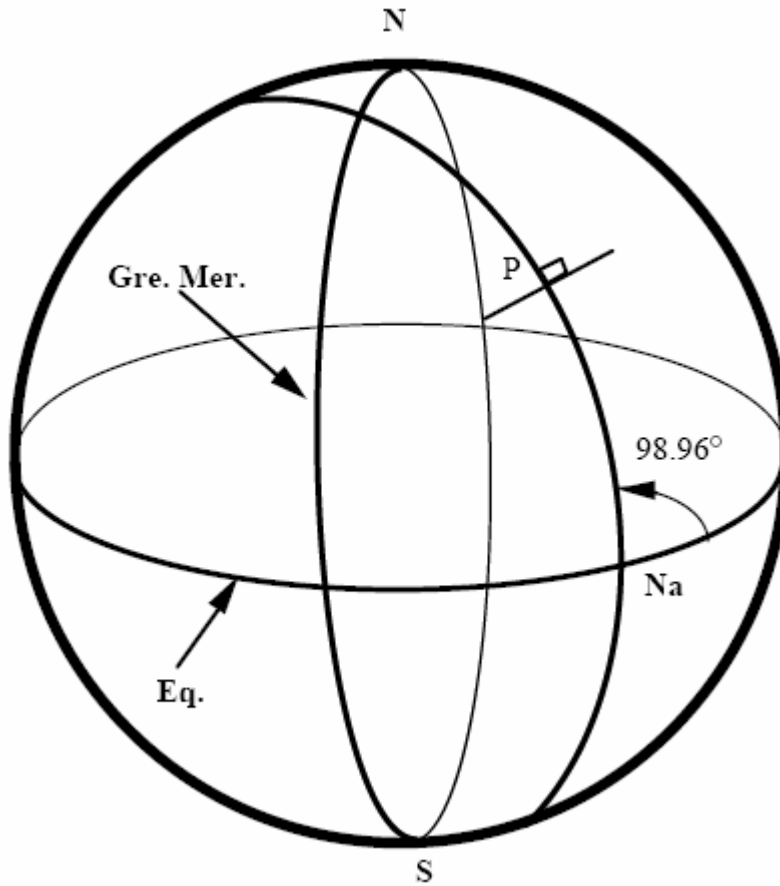


Fig. 1.

Let $\dot{\lambda}_N$ be the hour movement in rad/sec, H_N the hour at the ascendant node, λ_N its longitude and N_c the pixel number.

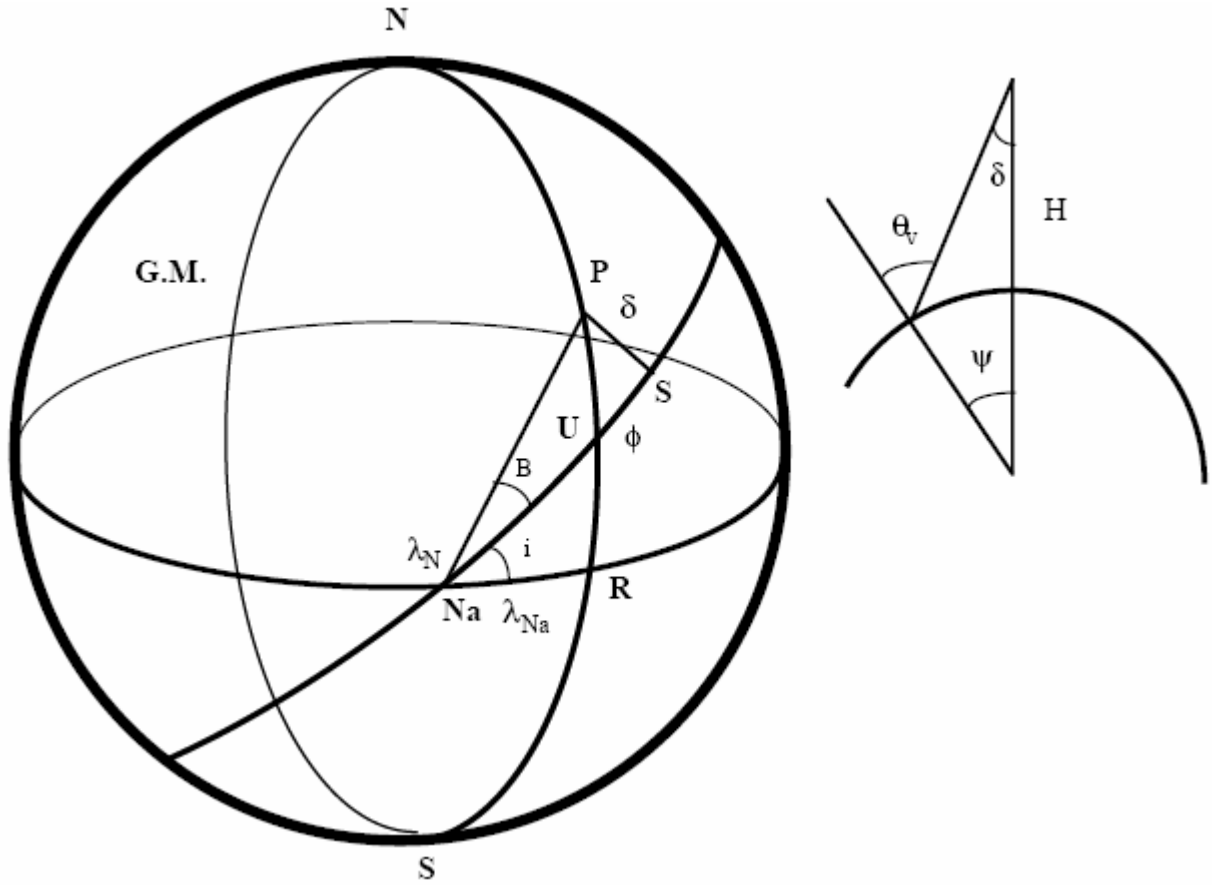


Fig. 2.

Lets consider Fig. 2. S is the subsatellite point, N is the ascendant node and P is the observed point. The scan angle δ gives an angle noted ψ at the centre of the Earth.

By solving the triangle PRN, we have the latitude ϕ_p so that:

$$\sin \phi_p = \sin(i + B) \sin(NP) .$$

Now, in triangle PSN

$$\sin(NP) = \sin \psi / \sin B$$

and

$$\tan(B) = \tan \psi / \sin U .$$

So,

$$\sin \phi_p = \cos i \sin \psi + \sin i \cos \psi \sin U .$$

By solving PRN, we obtain the longitude λ_p with respect to λ_N :

$$\sin \lambda_p = \sin NPR \sin NP$$

with

$$\sin \text{NPR} = \frac{\cos(i + B)}{\cos \phi_p}.$$

So, we write

$$\sin \lambda_p = \frac{\cos(i + B) \sin \text{NP}}{\cos \phi_p}$$

or

$$\sin \lambda_p = \frac{\cos(i + B) \sin \psi}{\cos \phi_p \sin B} = \frac{-\sin i \sin \psi + \cos \psi \cos i \sin U}{\cos \phi_p}.$$

To completely determine the longitude, we use the other relation which gives the cosine

$$\cos \lambda_p = \frac{\cos \psi \cos U}{\cos \phi_p}$$

The absolute longitude (Greenwich, Meridian reference) is given by

$$\lambda = \lambda_p + \lambda_N - (T - H_{Na}) \frac{2\pi}{86400}$$

where T is the time of the acquisition; the last term is needed to take into account the rotation of the Earth between T and H_{Na} . Let us recall that the movement angle U is calculated from $U = AN \cdot (T - H_{Na})$.

Consider again Fig. 2 to determine the observation azimuth and zenith angles.

δ is defined as

$$\delta = 55.385 \frac{N_c - 1024}{1024} \quad \text{in deg.},$$

the view zenith angle θ_v is defined by

$$\theta_v = a \sin \left[\left(1 + \frac{H}{R} \right) \sin \delta \right]$$

The observation azimuth angle ϕ_v is determined by solving the triangle NSP,

$$\sin \phi_v = \frac{\sin(\lambda_s - \lambda_p) \cos \phi_s}{\sin \psi}$$

and

$$\cos \phi_v = \frac{\sin \phi_s - \sin \phi_p \cos \psi}{\cos \phi_p \sin \psi},$$

where ϕ_s and λ_s are the latitude and longitude of the sub-satellite point P.

Reference:

The characteristics of the orbit have been taken from:

NOAA Polar Orbiter Data Users Guide, 1985, U.S. Department of Commerce, NOAA: National Environment Satellite, National Climatic Data Center, Satellite Data Service Division, World Weather Building, Room 100, Washington DC 20233, USA.

SUBROUTINE POSSOL

Function: To compute the solar azimuth and zenith angles (in degrees) for a point over the globe defined by its longitude and latitude (in dec. degrees) for a day of the year (fixed by number of the month and number of the day in the month) at any Greenwich Meridian Time (GMT dec. hour).

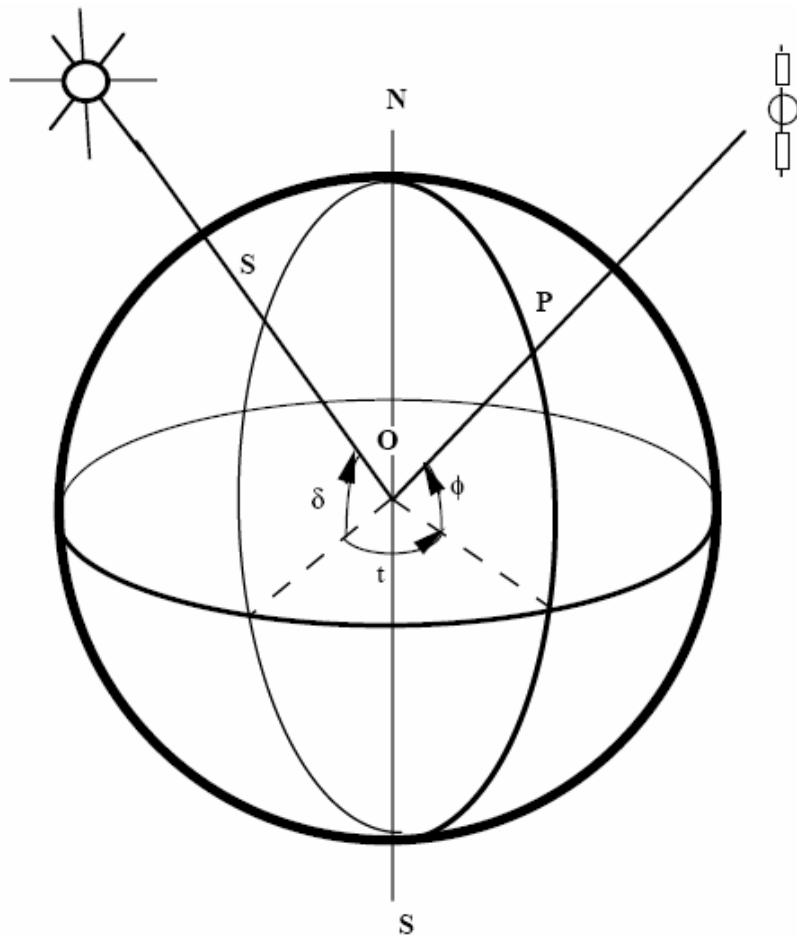


Fig.1.

Description: Let P be the point determined by the latitude ϕ and the declination of the sun δ at this period of the year, the hour angle is noted as t. So the incident angle θ_s can be determined by the spherical trigonometry expression

$$\cos \theta_s = \cos\left(\frac{\pi}{2} - \delta\right) \cos\left(\frac{\pi}{2} - \phi\right) + \sin\left(\frac{\pi}{2} - \delta\right) \sin\left(\frac{\pi}{2} - \phi\right) \cos t$$

or

$$\cos \theta_v = \sin \delta \sin \phi + \cos \delta \cos \phi \cos t .$$

The solar declination depends upon the day of the year. We used the decomposition in Fourier series of the declination based on astronomical data with the expression:

$$\delta = \beta_1 - \beta_2 \cos(A) + \beta_3 \sin(A) - \beta_4 \cos(2A) + \beta_5 \sin(2A) - \beta_6 \cos(3A) + \beta_7 \sin(3A)$$

where $A = \frac{2\pi J}{365}$ and J is the Julian day

$$\begin{aligned} \beta_1 &= .006918, \beta_2 = .399912, \beta_3 = .070257, \beta_4 = .006758, \\ \beta_5 &= .000907, \beta_6 = .002697, \beta_7 = .001480 \end{aligned}$$

The hour angle is computed from the following considerations. From the GMT time, we compute the mean solar time (or local time) for the longitude λ

$$\text{MST} = \text{GMT} + \frac{\lambda}{15} \text{ (dec.hour)}$$

The length of the day changes within the year (differences between +30 s and -20 s), so we have to correct the local time to obtain the true solar time (TST)

$$\text{TST} = \text{MST} + \text{ET},$$

where the equation of time ET is given by:

$$\text{ET} = \frac{(\alpha_1 + \alpha_2 \cos(B) - \alpha_3 \sin(B) - \alpha_4 \cos(2B) - \alpha_5 \sin(2B))12}{\pi} \text{ (dec.hour)}$$

with

$$B = \frac{2\pi J}{365}, \alpha_1 = .000075, \alpha_2 = .001868, \alpha_3 = .032077, \alpha_4 = .014615, \alpha_5 = .040849$$

We obtain the hour angle t

$$t = 15 \frac{\pi}{180} (\text{TST} - 12) \text{ (radians)}$$

and can compute θ_s .

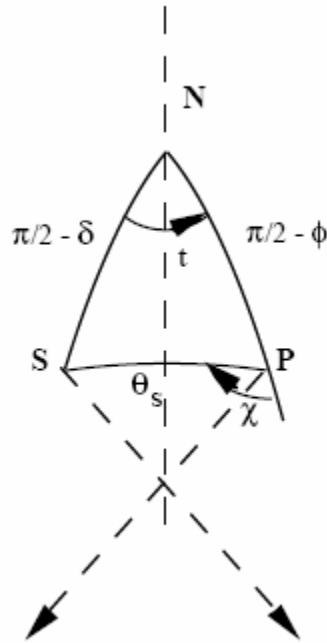


Fig. 2.

To determine the azimuth angle ϕ_s , we solve the spherical triangle NSP

$$\frac{\sin \chi}{\sin\left(\frac{\pi}{2} - \delta\right)} = \frac{\sin t}{\sin \theta_s}$$

where χ is the solar azimuth angle measured from the south through the west,

Or

$$\sin \chi = \cos \delta \frac{\sin t}{\sin \theta_s}.$$

To determine the sign of χ we use the cosine

$$\cos \chi = \frac{\cos \phi \sin \delta + \cos \delta \cos t}{\sin \theta_s},$$

so χ is completely defined.

To define the solar azimuthal angle ϕ_s with respect to the North, we write,

$$\phi_s = \pi + a \sin \chi$$

References:

Ch. Perrin de Brichambaut, Rayonnement solaire et échanges radiatifs naturels, *Monographies de météorologie*, Gauthier-Villars, Paris, France, 1963.

N. Robinson, Solar Radiation, Elsevier Publishing Company, New-York, N.Y., 10017, 1966.

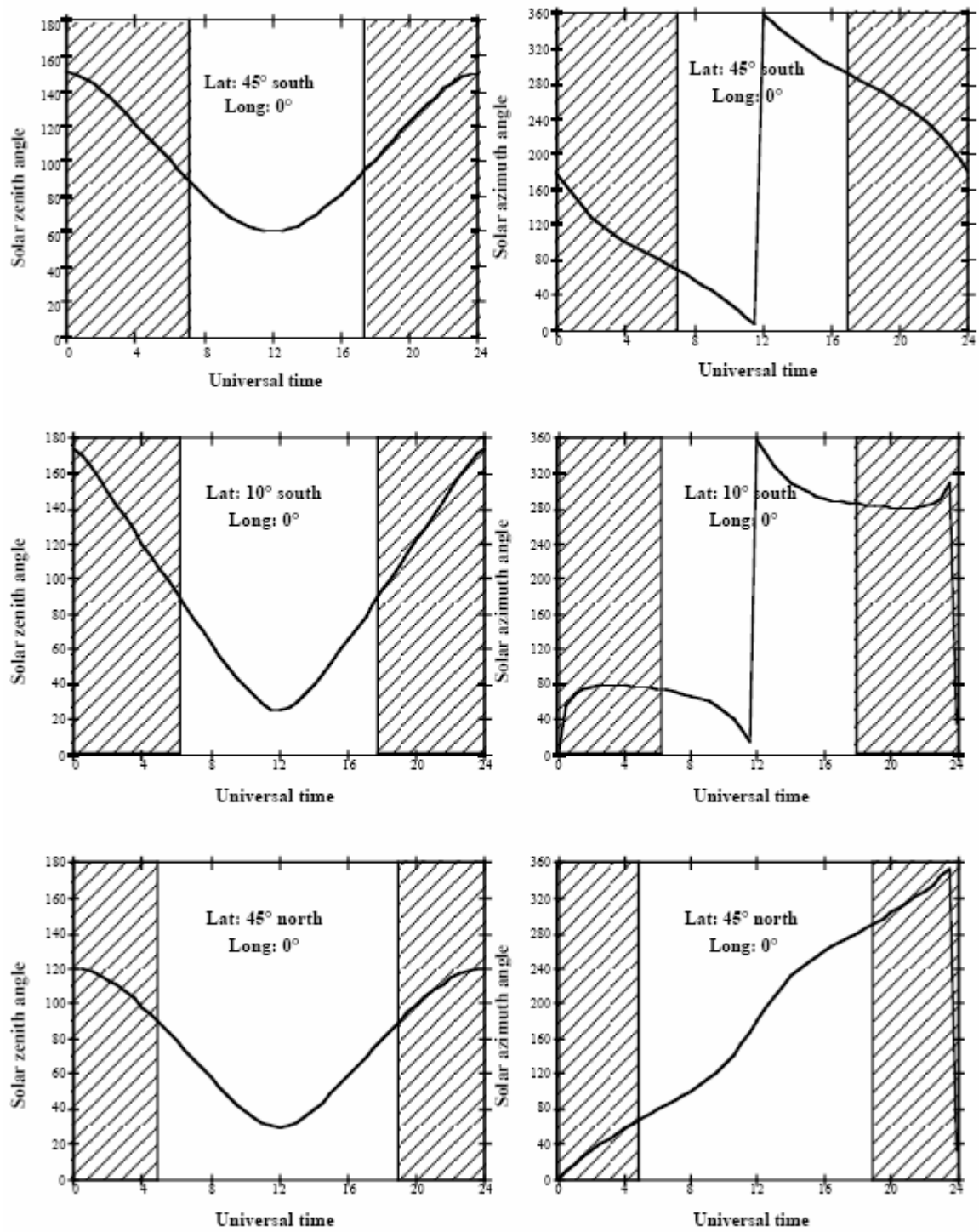


Fig. 3. Simulation of solar angles for the 1st of May, at different latitudes, vs. Universal Time.

SUBROUTINE POSSPO

Function: To compute the geometrical conditions for the SPOT satellite. As the dimensions of the frame are 60×60 km with an observation angle of maximum 2.06° , we have considered that:

- the observation zenith angle is nul, so the azimuth angle is not defined,
- the incident conditions are the same that those computed for the center of the frame.

Note: We have not considered the off-nadir viewing.

Reference:

M. Chevrel, M. Courtois, and G. Weill, The SPOT satellite remote sensing mission, *Photogrammetric Engineering and Remote Sensing*, 47, 1163-1171, 1981.

DESCRIPTION OF THE SUBROUTINES USED

TO COMPUTE THE ATMOSPHERIC CONDITIONS

SUBROUTINE ABSTRA

Function: To compute the gaseous transmittance between 0.25 and 4 μm for downward, upward and total paths. We consider six gases (O_2 , CO_2 , H_2O , O_3 , N_2O , and CH_4) separately. The total transmission is put equal to the simple product of each ones. The spectral resolution is equal to 10 cm^{-1} .

Description: We have used two random exponential band models (*Goody* for H_2O and *Malkmus* for O_2 , CO_2 , O_3 , N_2O , and CH_4) to compute the gaseous transmissions. If we consider a homogeneous path, the transmission function is written for H_2O

$$t_{\Delta\nu}^G = \exp\left[-\frac{N_0 k m}{\Delta\nu} \left(1 + \frac{k m}{\pi\alpha_0}\right)^{-1/2}\right], \quad (1)$$

for the other gases

$$t_{\Delta\nu}^M = \exp\left[-\frac{2\pi\alpha_0 N_0}{\Delta\nu} \left(\left(1 + \frac{k m}{\pi\alpha_0}\right)^{-1/2} - 1\right)\right], \quad (2)$$

where m is the absorber amount, N_0 is the total line number in the frequency interval $\Delta\nu$, k is the average intensity and α_0 is the average *Lorentz* half width, obtained from the intensity S_j and half width α_j of the j^{th} spectral line by

$$k = \frac{\sum_{j=1}^{N_0} S_j}{N_0} \quad (3)$$

$$\frac{k}{\pi\alpha} = \frac{1}{4} \left[\frac{\sum_{j=1}^{N_0} S_j}{\sum_{j=1}^{N_0} (S_j \alpha_j)^{1/2}} \right]^2 \quad (4)$$

The spectral resolution of 10 cm^{-1} is sufficient and contains enough spectral lines to use a random band model transmission function.

From a general point of view, the width of a spectral line corresponds to the convolution product of the two shapes, *Lorentz* and *Doppler*, and is therefore called a *Voigt* line. For an

atmospheric gas (O₂, CO₂, H₂O, O₃, N₂O, and CH₄), the altitude where the *Lorentz* width and *Doppler* width are equivalent is about 30 km. So, according to the vertical distribution, only O₃ requires a more complex treatment to take into account a *Voigt* profile. The O₃ visible transmission is computed by another method detailed in the next part and the absorption in the solar infrared (3.3 μm) is very small (see Fig. I-2 of Part I of the manual). Therefore, we have used the same formalism for all gases. The approximation contributes no consequential error.

Equations (1) and (2) are valid for a homogeneous path, where pressure and temperature are assumed to be constant. To take into account the variations of temperature and pressure along the atmospheric path, we use the *Curtis-Godson* approximation which associates an amount \bar{m} weighted by temperature (thereby related to the line intensity), and a amount $\overline{m\phi}$ weighted by pressure and temperature (thereby related to the intensity and half width line)

$$\bar{m}(z, z') = \int_z^{z'} \Phi(T) du \quad (5)$$

$$\overline{m\phi}(z, z') = \int_z^{z'} \Psi(T)\phi du \quad (6)$$

with

$\phi = p/p_0$ (p_0 is the standard pressure at which the measurements of spectroscopic parameters were made), and

$du = \rho_g (dz/\mu)$ (ρ_g is the gaseous density and μ is the cosine of the viewing angle).

The functions $\Phi(T)$ and $\Psi(T)$ are given by

$$\Phi(T) = \frac{\sum_{j=1}^{N_0} S_j(T)}{\sum_{j=1}^{N_0} S_j(T_r)}, \quad (7)$$

$$\Psi(T) = \left[\frac{\sum_{j=1}^{N_0} [S_j(T)\alpha_{j0}(T)]^{1/2}}{\sum_{j=1}^{N_0} [S_j(T_r)\alpha_{j0}(T_r)]^{1/2}} \right]^2, \quad (8)$$

where T_r is the reference temperature, α_{j0} is the half-width at temperature T_r , and p_0 is the pressure.

To simplify, we fit these functions with

$$\Phi(T) = \exp[a(T - T_r) + b(T - T_r)^2], \quad (9a)$$

$$\Psi(T) = \exp[a'(T - T_r) + b'(T - T_r)^2]. \quad (9b)$$

The spectroscopic data are taken from the *AFGL* atmospheric absorption line parameters compilation (1991 edition). We have selected the following parameters:

- the position (in cm^{-1}),
- the integrated line strength $S_j(T_r)$ at 296 K (in $\text{cm}^{-1}/(\text{molecules cm}^2)$),
- the half width α_{j0} at 296 K and 1013 mb (in cm^{-1}),
- the energy of the lower transition state.

The half width at any temperature and pressure is obtained by

$$\alpha_j(p, T) = \alpha_{j0} \left(\frac{p}{p_0} \right) \left(\frac{T_r}{T} \right)^{1/2}, \quad (10)$$

and the intensity at any temperature can be computed from the vibrational and rotational partition and the energy of the lower transition state.

Subsequently, we have taken $T_r = 250$ K and computed $\Phi(T)$ and $\Psi(T)$ for 3 temperatures (200, 250 and 300 K) to determine the coefficients a , a' , b and b' .

Now we have a series of eight coefficients by steps of 10 cm^{-1} :

$$\bullet \quad \frac{k}{\delta} = \frac{\sum_{j=1}^{N_0} S_j(T_r)}{\Delta v} \quad (11)$$

$$\bullet \quad \frac{\pi\alpha_0}{\delta} = \frac{4}{\Delta v} \frac{\left[\sum_{j=1}^{N_0} [S_j(T_r)\alpha_{j0}(T)]^{1/2} \right]^2}{\sum_{j=1}^{N_0} S_j(T_r)} \quad (12)$$

- a, a'
- b, b'
- v_{low} the lower frequency of the interval, and $v_{\text{sup}} = v_{\text{low}} + 10\text{cm}^{-1}$

These coefficients are read in the subroutines, WAVA1 to 6 for H_2O , OZON1 for O_3 , OXYG3 to 6 for O_2 , and DICA1 to 3 for CO_2 .

The weighted absorber amounts \overline{m} and $\overline{m\phi}$, computed according to Eqs. (5) and (6) and the transmission functions (which correspond to Eqs. (1)-(2) for a homogeneous path), are written as

$$t_{\Delta v}^G = \exp \left[-\frac{k \bar{m}}{\delta} \left(1 + \frac{k \bar{m}^2}{\pi \alpha_0 \bar{m} \phi} \right)^{-1/2} \right] \quad (13)$$

$$t_{\Delta v}^M = \exp \left[-\frac{\pi \alpha_0 \bar{m} \phi}{\delta} \frac{1}{2 \bar{m}} \left(\left(1 + \frac{4k \bar{m}^2}{\pi \alpha_0 \bar{m} \phi} \right)^{-1/2} \right) \right] \quad (14)$$

Due to the deficiency of spectroscopy data, the visible ozone transmission function is written as

$$t_{O_3}(\Delta v) = \exp(-A_{O_3}(\Delta v)u_{O_3}) \quad (15)$$

where u_{O_3} is the absorber amount and A_{O_3} is the absorption coefficient given by *Kneizys et al.* (1980). These coefficients are given in steps of 200 cm^{-1} between 13000 and 24200 cm^{-1} and by step of 500 cm^{-1} between 27500 and 50000 cm^{-1} .

To take into account the water vapor continuum, we use the same expression with the coefficients A_{H_2O} given in steps of 5 cm^{-1} between 2350 and 2420 cm^{-1} .

A comparison between MODTRAN2 and our results (6S) is shown in the Fig. 1-3. The difference observed at roughly $3.1 \mu\text{m}$ is due to the fact that we have not taken into account the N_2O continuum. This spectral range is already contaminated by water vapor and is not an atmospheric window. Therefore, the $3.1 \mu\text{m}$ region is not used in remote sensing and its emission in 6S generally unimportant.

References:

- A.R. Curtis, The computation of radiative heating rates in the atmosphere, *Proceedings of the Royal Society of London*, A236, 156-159, 1956.
- R.G. Ellingson and J.C. Gille, An infrared radiative transfer model. Part 1: Model description and comparison of observations with calculations, *Journal of the Atmospheric Sciences*, 35, 523-545, 1978.
- R.M. Goody, Atmospheric radiation: 1. Theoretical basis, Oxford University Press, 436p, 1964.
- F.X. Kneizys, E.P. Shettle, W.O. Gallery, J.H. Chetwynd, Jr., L.W. Abreu, J.E.A. Selby, R.W. Fenn, and R.A. Mc Clatchey, Atmospheric transmittance/radiance: Computer code LOWTRAN 5, AFGL-TR-80-0067, Air Force Geophysics Laboratory, Bedford, MA, 1980.
- W. Malkmus, Random Lorentz band model with exponential-tailed S^{-1} line-intensity distribution function, *Journal of the Optical Society of America*, 57, 3, 323-329, 1967.

J.J. Morcrette, Sur la paramétrisation du rayonnement dans les modèles de la circulation générale atmosphérique, Thèse d'Etat no 630, Université de Lille.

D.C. Robertson, L.S. Bernstein, R. Haimes, J. Wunderlich, and L. Vega, 5 cm^{-1} band model option to Lowtran 5, *Applied Optics*, 20, 3218-3226, 1981.

C.D. Rodgers and C.O. Walshaw, The computation of infrared cooling rates in planetary atmospheres, *Quarterly Journal of the Royal Meteorology Society*, 92, 67-92, 1966.

L.S. Rothman, R.R. Gamache, A. Barbe, A. Goldman, J.R. Gillis, L.R. Brown, R.A. Toth, J.M. Flaud, and C. Camy-Peyret, AFGL atmospheric absorption line parameters compilation: 1982 Edition, *Applied Optics*, 22, 2247-2256, 1983.

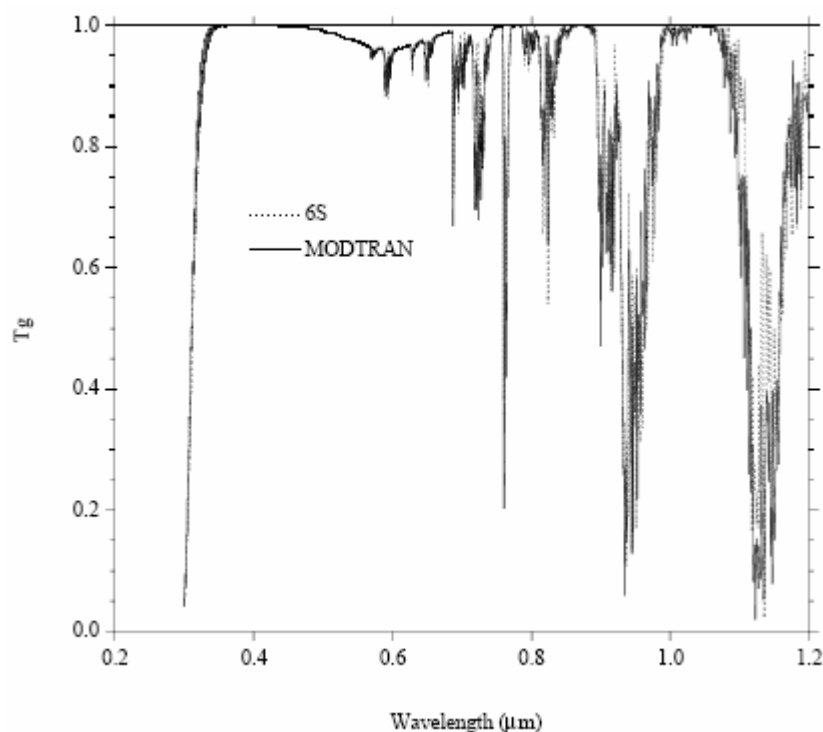


Fig. 1. Gaseous transmission between 0.25 and 1.25 μm (mid. lat. summer atmosphere).

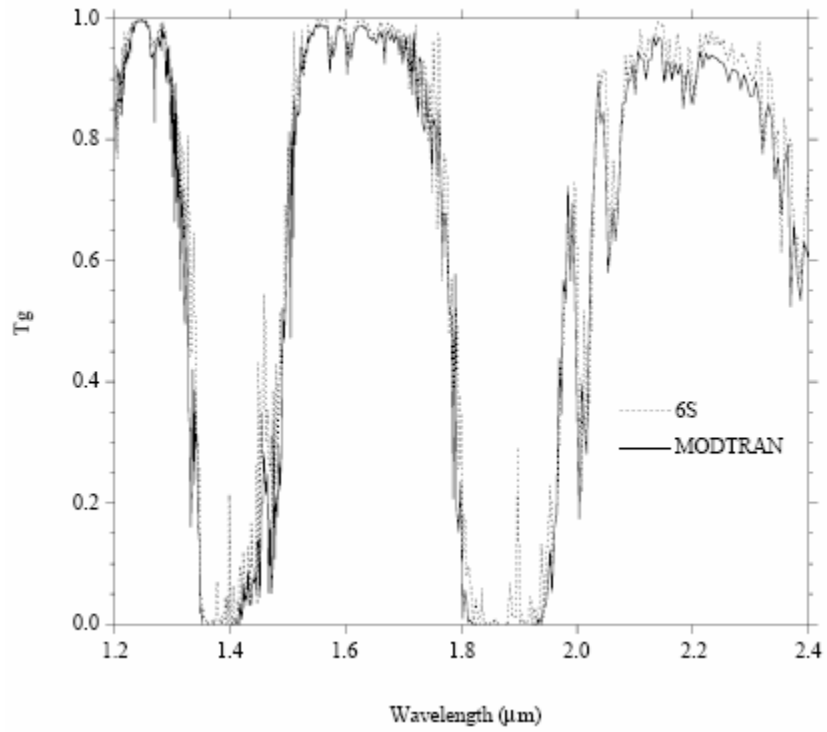


Fig. 2. Gaseous transmission between 1.20 and 2.40 μm (mid. lat. summer atmosphere).

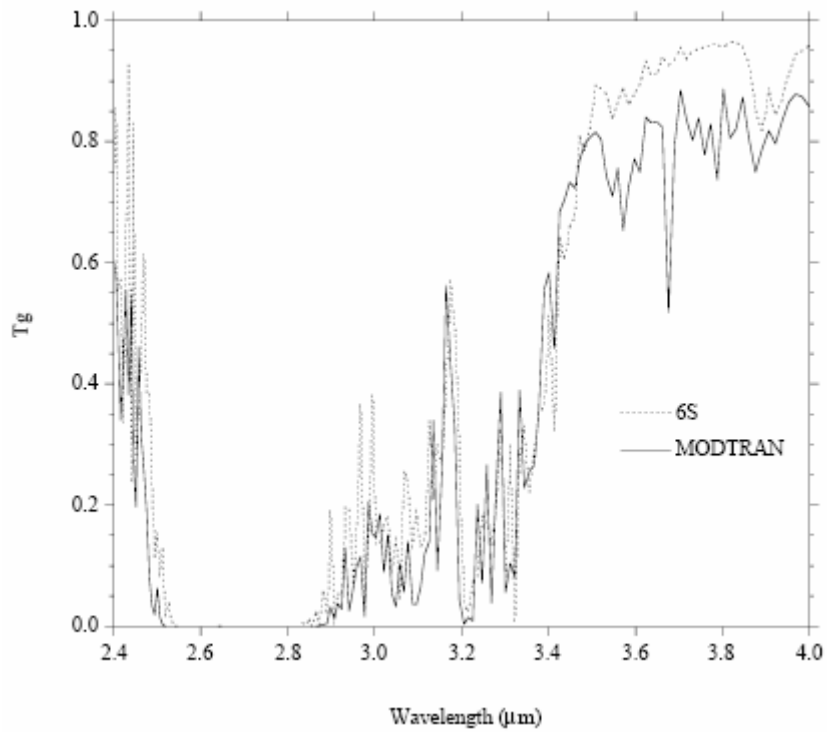


Fig. 3. Gaseous transmission between 2.40 and 4.00 μm (mid. lat. summer atmosphere).

SUBROUTINE AEROSO

Function: To compute the optical scattering parameters (extinction and scattering coefficients, single scattering albedo, phase function, and asymmetry factor) at the 20 discrete wavelengths for an aerosol model selected (or created) from:

(1) the characteristics of the basic components (*Lenoble, 1984; d’Almeida, 1991*).

- dust-like component (D.L., subroutine DUST)
- oceanic component (O.C., subroutine OCEA)
- water-soluble component (W.S., subroutine WATE)
- soot component (S.C., subroutine SOOT)

(2) pre-computed characteristics of

- biomass burning smoke model (subroutine BBM, *Dubovik et al., 2002*)
- stratospheric aerosol model (subroutine BDM, *d’Almeida et al., 1991*)
- background desert model (subroutine STM, *Russel et al., 1996*)

(3) computed using the MIE theory with inputs (size distribution, refractive indexes...) given by the user (see subroutine MIE (and EXSCPHASE)).

Description: From the Mie theory (see subroutine MIE), we have computed the phase function $P(\Theta)$, the extinction and scattering coefficients, the asymmetry factor g for the basic components defined by their size distributions and refractive indices. The computations were performed at 20 wavelengths and 83 phase angles (80 Gauss angles, 0° , 90° and 180°) by default or up to 1000 phase angles (997 Gauss angles, 0° , 90° and 180°) specified by the user.

From the four basic components, three tropospheric aerosols types models can be created by mixing with the following volume percentages. By “mixing”, we assume an idea of "external mixing" in the model construction, so the resultant values are obtained by a weighted average using the volume percentages C_j given by:

	D.L.	W.S.	O.C.	S.C.
Continental	0.70	0.29		0.01
Maritime		0.05	0.95	
Urban	0.17	0.61		0.22

For each component, we computed the volume concentration V_j and the particle number concentration N_j (particle/cm³) using the Log-Normal distribution:

	D.L.	W.S.	O.C.	S.C.
$V_j, \mu^3/\text{cm}^3$	113.98352	$113.98352 \cdot 10^{-06}$	5.14441	$59.777553 \cdot 10^{-06}$
$N_j, \text{part}/\text{cm}^3$	54.73400	$1.86850 \cdot 10^{06}$	276.0500010	$1.86850 \cdot 10^{06}$

where

$$V_j = \frac{4\pi}{3} \int_0^{+\infty} r^3 \frac{dN_j(r)}{dr} dr$$

and N_j is computed in such a way that the extinction coefficient is normalized at 550 nm.

If C_j is the aerosol fraction by volume of the component j , we have $C_j = v_j/v$ with $v_j = n_j V_j$, where n_j is the number of particles in the mixing, so

$$n = \sum_j n_j = v \sum_j \frac{C_j}{V_j}$$

Then we can obtain the percentage density of particles

$$\frac{n_j}{n} = \frac{\frac{C_j}{V_j}}{\sum_j \frac{C_j}{V_j}}$$

so, for example, n_j/n for the 3 selected models:

	D.L.	W.S.	O.C.	S.C.
Continental	$2.26490 \cdot 10^{-06}$	0.938299		0.0616987
Maritime		0.999579	$4.20823 \cdot 10^{-04}$	
Urban	$1.65125 \cdot 10^{-07}$	0.592507		0.407492

To obtain the extinction coefficient of the resultant model, we compute

$$K^{\text{ext}}(\lambda) = \sum_j \frac{n_j}{n} K_j^{\text{ext}}(\lambda)$$

and we also normalize this coefficient at 550 nm. So we have to compute the equivalent number N of particles by

$$N = \frac{1}{\sum_j \frac{n_j}{n} K_j^{\text{ext}}(550)}.$$

Since $K_j^{\text{ext}}(550) = 1/N_j$, we obtain

$$\frac{1}{N} = \sum_j \frac{n_j}{n} \frac{1}{N_j}$$

The other optical parameters are computed by the same way:

- scattering coefficient

$$K^{\text{sca}}(\lambda) = N \sum_j \frac{n_j}{n} K_j^{\text{sca}}(\lambda),$$

- asymmetry factor

$$g(\lambda) = \frac{N}{K^{\text{sca}}(\lambda)} \sum_j \frac{n_j}{n} g_j(\lambda) K_j^{\text{sca}}(\lambda),$$

- phase function

$$P_\lambda(\Theta) = \frac{N}{K^{\text{sca}}(\lambda)} \sum_j \frac{n_j}{n} P_\lambda^j(\Theta) K_j^{\text{sca}}(\lambda),$$

- the single scattering albedo is directly obtained by the ratio

$$\omega_0(\lambda) = \frac{K^{\text{sca}}(\lambda)}{K^{\text{ext}}(\lambda)}.$$

Notes:

- The data for extinction or scattering coefficients are in km^{-1}
- The following figures give us an order of magnitude of these terms for the 3 selected aerosol models plus the desert aerosol model.

References:

World Meteorological Organization (CAS)/Radiation Commission of IAMAP Meeting of experts on aerosols and their climatic effects, WCP 55, Williamsburg, Virginia, U.S.A., 28-30 March 1983.

O. Dubovik, B. Holben, T.F. Eck, A. Smirnov, Y.J. Kaufman, M.D. King, D. Tanré, and I. Slutsker, Variability of absorption and optical properties of key aerosol types observed in worldwide locations, *Journal of the Atmospheric Sciences*, 59, 590-608, 2002.

- G. A. d'Almeida, P. Koepke, and E. P. Shettle, Atmospheric aerosols: global climatology and radiative characteristics, A. DEEPAK Publishing, Hampton, Virginia, USA, 1991, p. 48, 80 and 120.
- P.B. Russel, J.M. Livingston, R.F. Pueschel; J.J. Bauman, J.B. Pollac, S.L. Brooks, P. Hamill, L.W. Thomason, L.L. Stowe, T. Deshler, E.G. Dutton, and R.W. Bergstrom, Global to microscale evolution of the Pinatubo volcanic aerosol derived from diverse measurements and analyses, *Journal of Geophysical Research*, 101 (D13), 18745-18763, 1996.

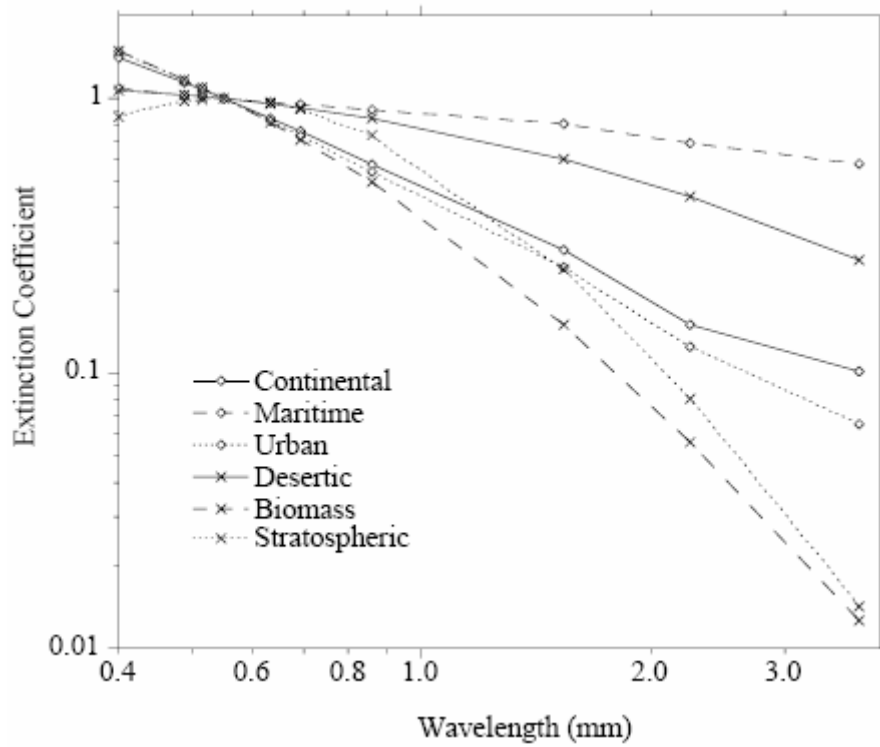


Fig. 1. Spectral dependence of the extinction coefficient for various aerosol models.

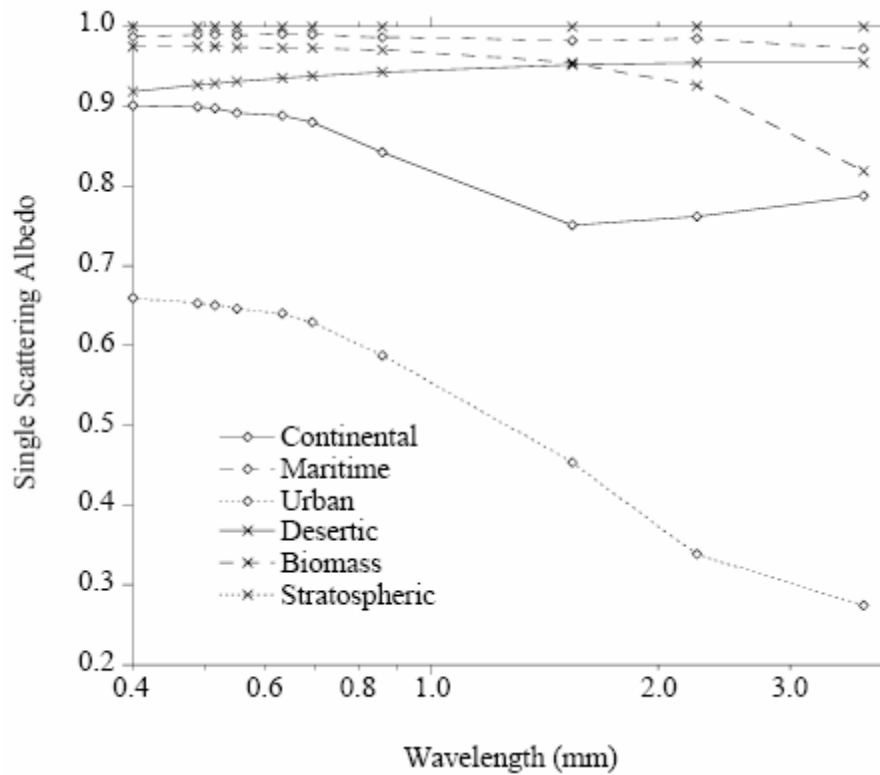


Fig. 2. Spectral dependence of the single scattering albedo for various aerosol models.

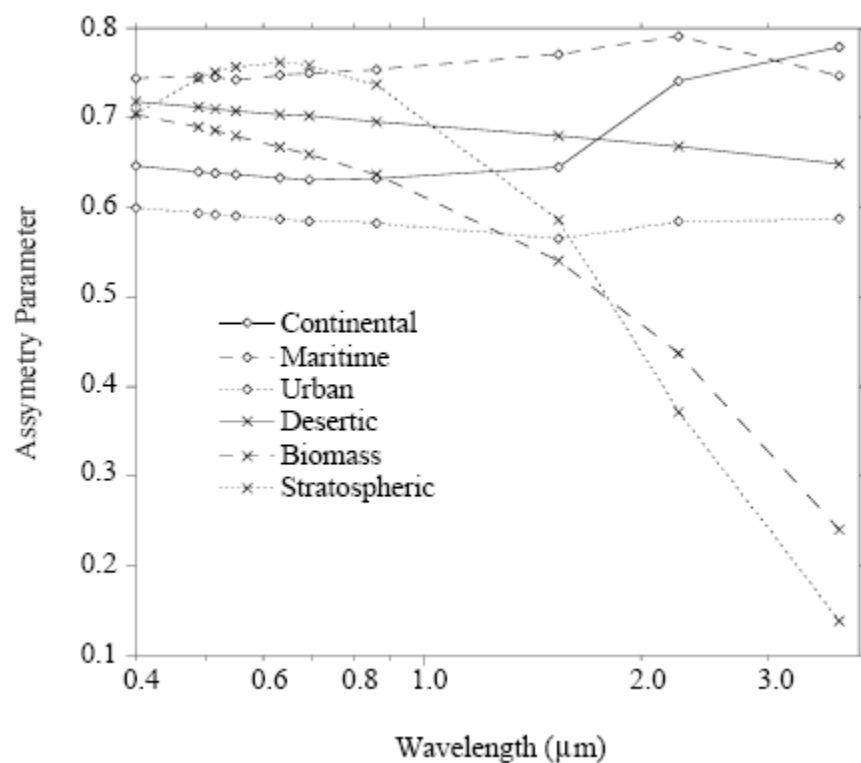


Fig. 3. Spectral dependence for the asymmetry parameter for various aerosol models.

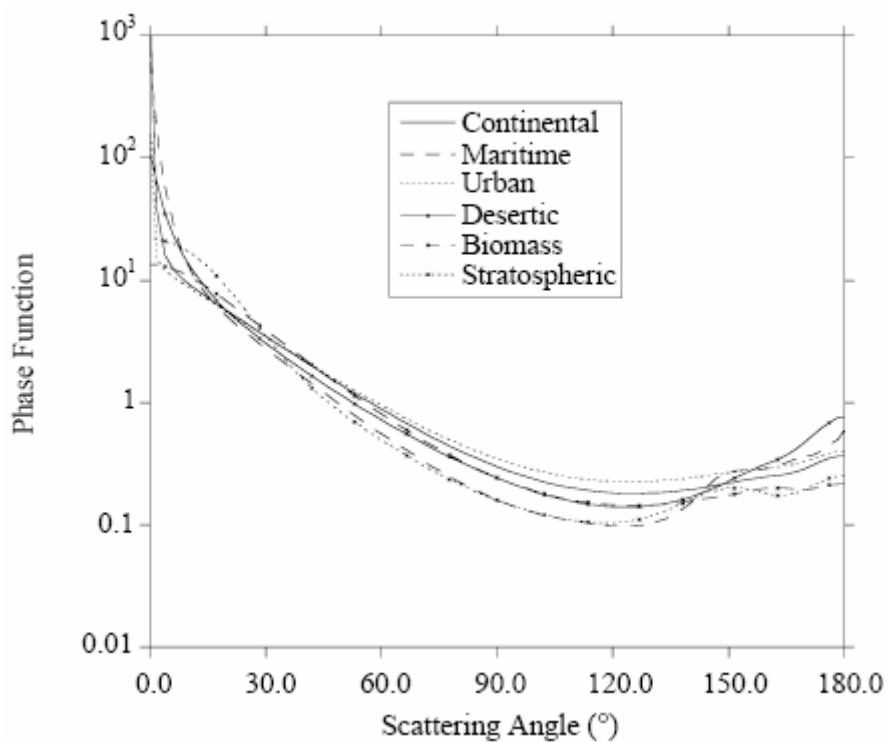


Fig. 4. Phase function at 550 μm versus scattering angle for various aerosol models.

SUBROUTINE AEROPROF

Function: To decompose the atmosphere into a finite number of calculation layers.

Description: For each calculation layer, AEROPROF calculates the optical thickness, layer height, proportion of molecules assuming an exponential vertical profile with the scale height of 8 km, and proportion of aerosol particles using the user-defined vertical profile. The maximum height of a user-defined aerosol atmosphere cannot exceed 300 km.

By its function, AEROPROF is analogous to the DISCRE subroutine, except for the fact that it incorporates the user-defined vertical aerosol profile.

SUBROUTINE ATMREF

Function: To compute the atmospheric reflectance for molecular, aerosol and mixed atmospheres. Computations are performed using the vector Successive Orders of Scattering method (see subroutine OSPOL).

Description: Three reflectance terms computed by ATMREF include the aerosol reflectance (ρ_A), rayleigh reflectance (ρ_R) and reflectance of a mixed Rayleigh-aerosol atmosphere (ρ_{R+A}). In addition, three different configurations of sensor position are possible, such as ground-based observation, satellite sensor and airborne sensor.

In case of ground-based observations, we consider that there is no contribution of the atmosphere below the sensor and the three reflectances are simply set to zero.

In case of satellite-based observations, we can consider that all molecules and aerosol particles are below the sensor. The subroutine OSPOL is used to compute the reflectances. This subroutine deals with purely molecular and aerosol atmospheres and with a mixture of molecules and aerosol particles by computing the signal in a set of layers for which the proportion of molecules and aerosol particles can be adjusted. The computation of the proportion of aerosol particles and molecules in each layer is optimized by the subroutine DISCRE, within which the entire atmosphere is divided into a number of layers with equal optical depths; the proportion depends on the aerosol profile, which is either assumed to be exponential with a scale height of 2 km or provided by the user.

In case of airborne observations, the three components are computed by the subroutine OSPOL. Within this subroutine, a special layer is set so that the top of the layer corresponds to the altitude of the aircraft. When the aerosol optical depth below the plane is provided by the user as encouraged, the aerosol scale height is computed again to match the total aerosol optical depth, aerosol optical depth below plane and plane altitude. If in this case the scale height is found to be greater than 7 km, a warning message is issued and computation are aborted.

References:

Radiation Commission of IAMAP, Standard procedures to compute atmospheric radiative transfer in a scattering atmosphere. Edited by J. Lenoble, Available from Dr. S. Ruttenberg, NCAR, Boulder Colorado 80307, U.S.A., 1977.

- D. Tanre, M. Herman, P.Y. Deschamps, and A. De Leffe, Atmospheric modeling for space measurements of ground reflectances including bidirectional properties, *Applied Optics*, 18(21), 3587-3594, 1979.
- J. L. Deuzé, M. Herman, and R. Santer, Fourier series expansion of the transfer equation in the atmosphere-ocean system. *Journal of Quantitative Spectroscopy and Radiative Transfer*, 41(6), 483 - 494, 1989.

SUBROUTINE CSALBR

Function: To compute the spherical albedo of the molecular layer.

Description: We integrate the transmission function of the different incident directions to calculate the spherical albedo, s , that is:

$$s = 1 - \int_0^1 \mu T(\mu) d\mu \quad (1)$$

Using the expression of $T(\mu)$ derived in SCATRA (Eq. (1)), it can be shown that s reduces to:

$$s = \frac{1}{4 + 3\tau} [3\tau - 4E_3(\tau) + 6E_4(\tau)] \quad (2)$$

where $E_3(\tau)$ and $E_4(\tau)$ are exponential integrals for the argument τ . These functions are easily computable from the expressions given in the reference below.

Figure 1 shows that the differences between the exact results and Eq. (2) are approximately 0.003 for $\tau = 0.35$ which results in an error of 0.0003 for a surface albedo of 0.10. In the red part of the solar spectrum for which the surface albedo may be larger, the error is still below 0.001.

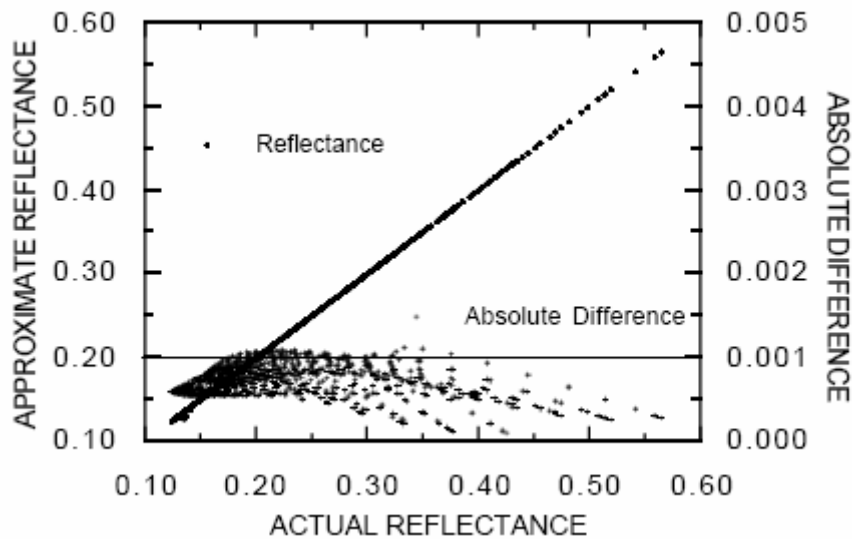


Fig. 1. Accuracy of Eq. (2).

Reference:

M. Abramowitz and I Stegun, Handbook of mathematical functions, New-York: Dover Publications, Inc., 1970.

SUBROUTINE DISCOM

Function: To compute optical properties of the atmosphere at 20 different wavelengths.

Description: 20 different wavelengths which fall within the atmospheric window used in remote sensing were selected as “node” wavelengths of the code.

$\lambda = \{0.350, 0.400, 0.412, 0.443, 0.470, 0.488, 0.515, 0.550, 0.590, 0.633, 0.670, 0.694, 0.760, 0.860, 1.240, 1.536, 1.650, 1.950, 2.250, 3.750\} \mu\text{m}$.

The computed parameters include

- molecular optical depth (subroutine ODRAYL)
- aerosol optical depth (subroutine ODA550)
- atmospheric reflectances (subroutine ATMREF)
- scattering transmittances (subroutine SCATRA)
- spherical albedos (subroutine SCATRA)

The computations are made for 3 types of the atmosphere:

- pure molecular
- pure aerosol
- mixed molecular and aerosol

SUBROUTINE DISCRE

Function: To decompose the atmosphere into a finite number of calculation layers.

Description: For each calculation layer, DISCRE calculates the optical thickness, layer height, and proportion of molecules and aerosol particles assuming an exponential vertical profile for each constituent. Figure 1 illustrates how molecules and aerosol particles are mixed in a realistic atmosphere. For molecules, the scale height is 8 km. For aerosol particles, it is assumed to be equal to 2 km unless specified otherwise by the user (using the ‘aircraft measurements’ option).

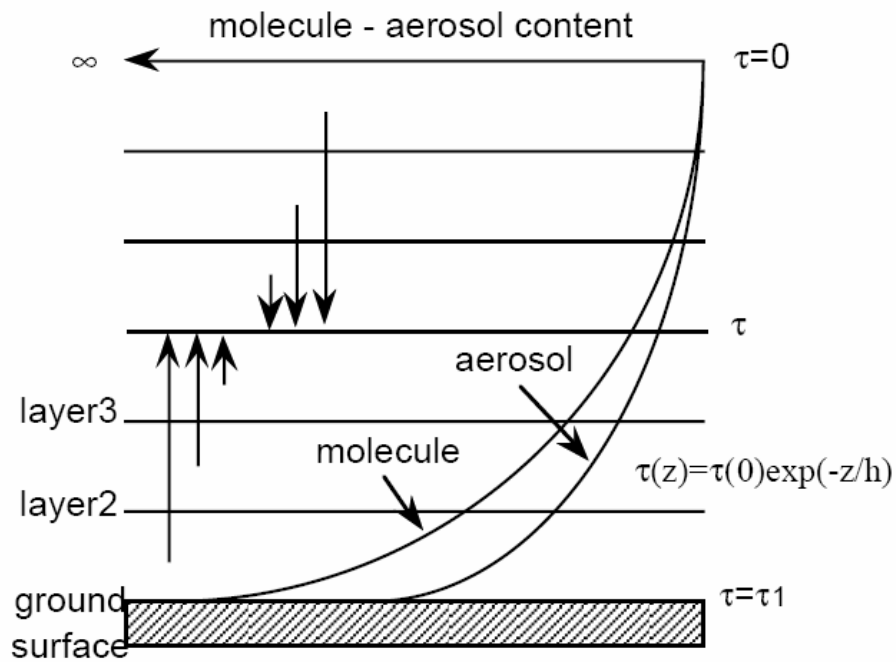


Fig. 1. Mixing of molecules and aerosol particles in a realistic atmosphere.

SUBROUTINE ENVIRO

Function: To compute the environment functions $F(r)$ which allows us to account for an inhomogeneous ground.

Description: For an accurate evaluation of $F(r)$, Monte Carlo computations are necessary to take into account

- the altitude dependence of the phase function
- the dependence of the phase function upon the aerosol type
- the scaling factors which are different for aerosol particles and molecule.

Simulations for some different vertical distributions and phase functions show that the variability of the environment function $F(r)$ can be rather tractable.

The molecular scattering which is a major factor for the enlarged contribution of the background can be linearized and accounted for by:

$$F(r) = \frac{t_d^R(\theta_v) F^R(r) + t_d^P(\theta_v) F^P(r)}{t_d^R(\theta_v) + t_d^P(\theta_v)} \quad (1)$$

where $t_d^R(\theta_v)$ and $t_d^P(\theta_v)$ are the diffuse fractions in the transmission functions respectively for Rayleigh and aerosols. $F^R(r)$ and $F^P(r)$ correspond to the environment functions estimated for Rayleigh and aerosols taken into account separately, these functions are slightly dependent upon the wavelength.

We have computed these two functions for a mean atmosphere at the satellite level (*Mc Clatchey et al.*, 1971) and we propose the following approximations:

$$F^P(r) = 1 - \left[0.448 E^{-0.27r} + 0.552 E^{-2.83r} \right] \quad (2)$$

$$F^R(r) = 1 - \left[0.930 E^{-0.08r} + 0.070 E^{-1.10r} \right], \quad (3)$$

where r is in km.

If the actual aerosol model (type and vertical distribution) does not differ much from the mean model, these approximations are reasonable and we account for major part of the environment effect. Figure 1 shows the two functions $F^R(r)$ and $F^P(r)$. We note that the horizontal scales of the environment effect are typically 1 km for aerosol scattering and 10 km for molecular scattering.

For the case of an airborne observation, we computed the altitude dependence of the

Rayleigh and aerosol environment function. For several typical altitude we have computed $F^R(r,z)$ and $F^P(r,z)$ by the Monte Carlo method and we have derived an approximate expression (Eqs. (2) and (3)). Figures 2 and 3 show the environment functions for the selected altitudes. For a plane flying at an arbitrary altitude, we perform a linear interpolation between the closest simulated altitudes in 6S to get the environment function at the altitude of the plane.

Effect of the view zenith angle

For 6S, we look at the dependence of these two environment functions as a function of the view zenith angle. Figures 4a and b show for several values of the view zenith angle the environment function of Rayleigh and aerosol. As it can be observed on Fig. 4a-b, there is a dependence of the function $F(r)$ on the view direction for the view zenith angle larger than 30° . In order to account for this effect, we chose to fit the environment function at the desired view angle solely as a function of the environment function computed for a nadir view, as it is suggested by Fig. 4a-b. The results presented on Fig. 4a-b (symbols) show that a simple polynomial function of nadir view environment function whose coefficients depend on the logarithm of the cosine of view angle is adequate. For molecules, the F function is fitted by the simple expression:

$$F_R(\theta_v) = F_R(\theta_v = 0^\circ) \cdot [\ln(\cos(\theta_v)) \cdot (1 - F_R(\theta_v = 0^\circ)) + 1] \quad (4)$$

for aerosol, a polynomial of a higher degree is needed, that is:

$$F_A(\theta_v) = F_A(\theta_v = 0^\circ) \cdot \left[\begin{array}{l} [1 + a_0 \ln(\cos(\theta)) + b_0 \ln(\cos(\theta))^2] + \\ F_A(\theta_v = 0^\circ) \cdot [a_1 \ln(\cos(\theta)) + b_1 \ln(\cos(\theta))^2] \\ F_A(\theta_v = 0^\circ)^2 \cdot [(-a_1 - a_0) \ln(\cos(\theta)) + (-b_1 - b_0) \ln(\cos(\theta))^2] \end{array} \right] \quad (5)$$

with $a_0=1.3347$, $b_0=0.57757$, $a_1=-1.479$, $b_1=-1.5275$

However, it has to be pointed out that if the approximations (Eqs. (4) and (5)) are capable of taking into account the adjacency effect for an arbitrary view angle, they implied uniformity of the background as a function of azimuth. As contributions of the adjacent pixels for a large view angle do not comply to the symmetry in azimuth, the 6S results, in case of large view angles, have to be interpreted more like a sensitivity test to the problem of adjacency effect rather than an actual way to perform the adjacency effect correction .

Reference:

D. Tanre, M. Herman, and P.Y. Deschamps, Influence of the background contribution upon space measurements of ground reflectance, *Applied Optics*, 20, 3676-3684, 1981.

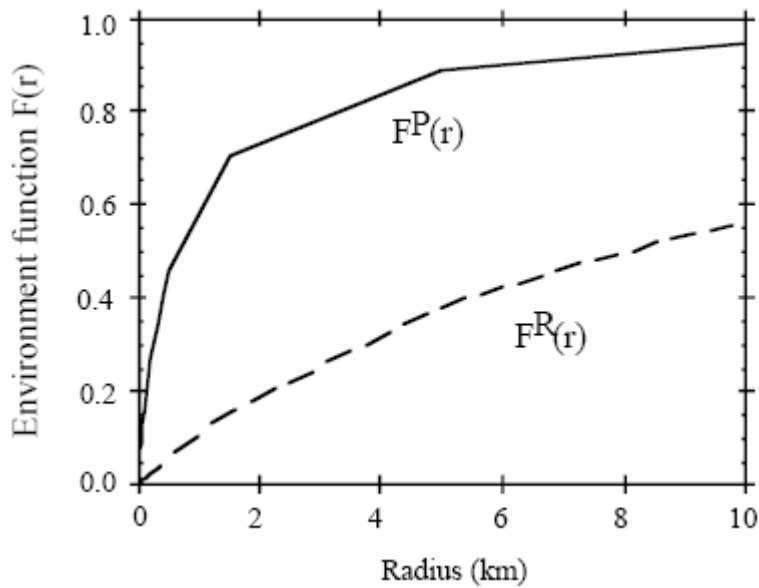


Fig. 1. Environment function at the satellite level for molecules and aerosol particles.

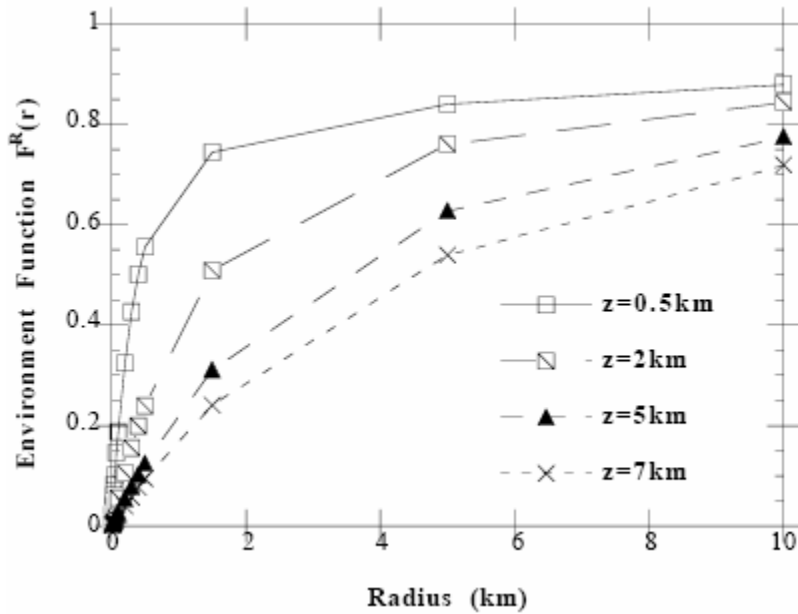


Fig. 2. Variation of the Rayleigh environmental function with the sensor altitude.

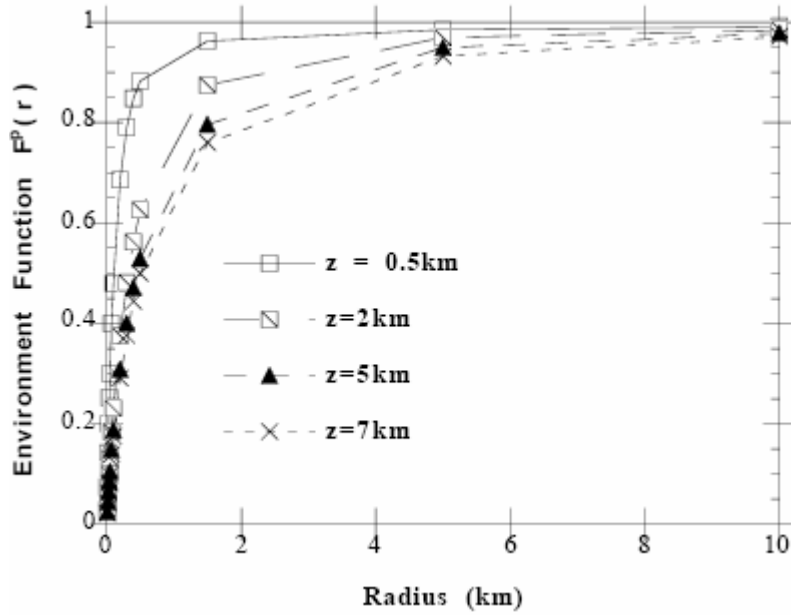


Fig. 3. Same as Fig. 2 but for particles.

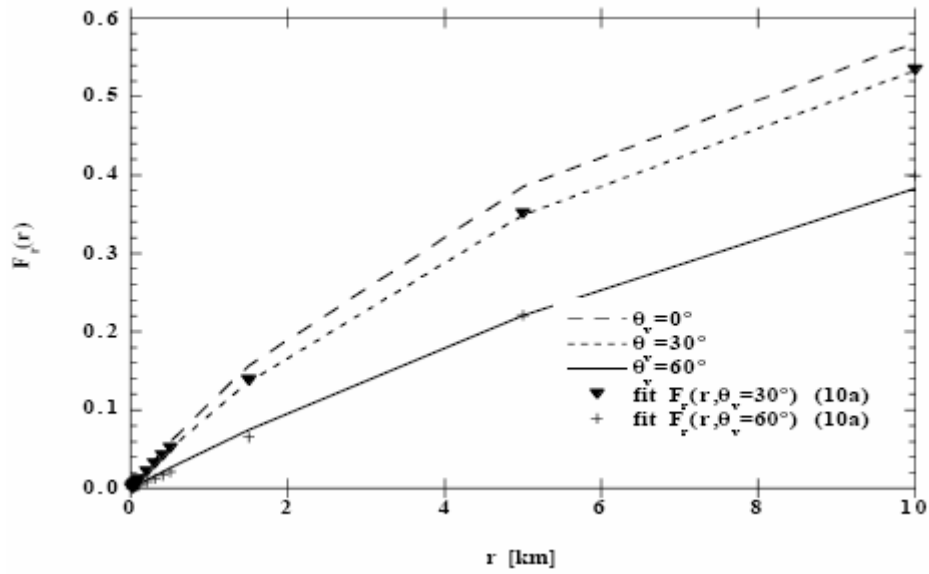


Fig. 4a. Environment function for a pure molecular atmosphere (lines) for different view zenith angle (θ_v) compared to the approximation used in 6S (symbols) as a function of the distance to the imaged pixel (r).

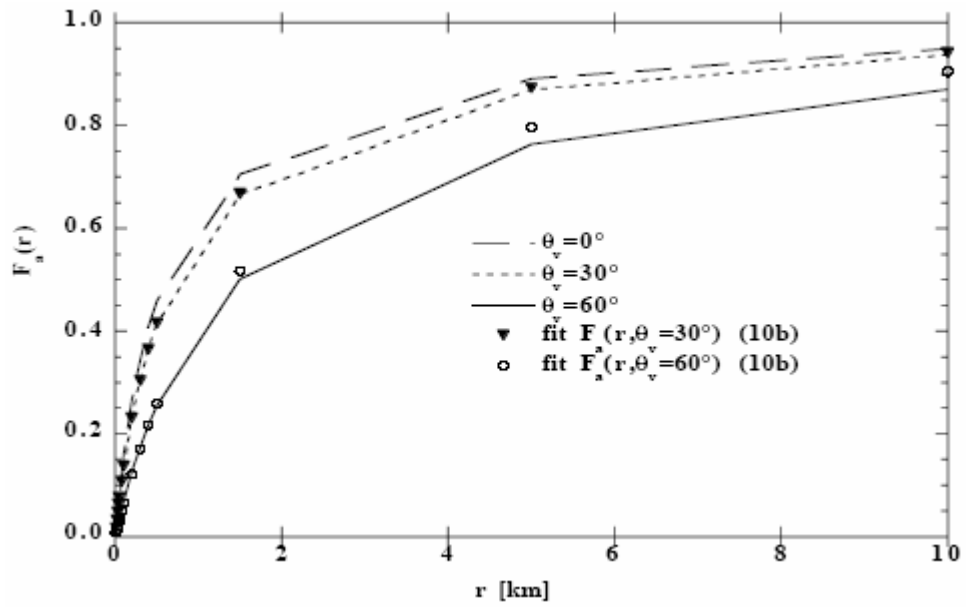


Fig. 4b. Same as Fig. 4a but for aerosol.

SUBROUTINE GAUSS

Function: To compute the Gaussian quadrature for a given number of angles n (Gaussian angles and their respective weights). The Gaussian quadrature is used in numerical integration involving the cosine of emergent or incident direction zenith angle.

SUBROUTINE INTERP

Function: To estimate the different atmospheric functions $\rho(\mu_s, \mu_v, \phi_s, \phi_v)$, $T(\theta)$ and S at any wavelength from the 20 discrete computations (subroutine DISCOM).

Description: The different atmospheric functions (noted f) have been assumed linear as a function of optical depth τ , so the interpolation scheme is written,

$$f(\tau) = A \lambda^{-\alpha}$$

The constants A and α are interpolated between 0.35 and 3.75 μm and extrapolated for the two extreme intervals 0.25–0.35 and 3.75–4 μm .

As the spectral dependences for Rayleigh ($\alpha = 4$) and aerosols ($\alpha = 1$) are quite different, we consider the two types of atmosphere separately.

SUBROUTINE ISO

Function: Compute the atmospheric transmission for either a satellite or aircraft observation as well as the spherical albedo of the atmosphere.

Description: The subroutine performs the computation on the basis of the Successive Orders of Scattering method (see subroutine OSPOL). The transmission is obtained directly by initially setting an isotropic source of radiation at the bottom of atmosphere. The spherical albedo is computed by numerical integration (Gaussian quadrature) of the transmission function (see Eq. (1) of subroutine CSALBR).

SUBROUTINE KERNEL

Function: Compute the values of Legendre polynomials used in the SOS (successive orders of scattering) method.

SUBROUTINE KERNELPOL

Function: The same as KERNEL, but including the polarization components of a scattering phase function.

SUBROUTINE MIE (and EXCPHASE)

Function: To compute, using the scattering of electromagnetic waves by a homogeneous isotropic sphere, the physical properties of particles whose sizes are comparable to or larger than the wavelength, and to generate a mixture of dry particles.

Description: The interaction of an electromagnetic wave with a absorbing sphere is described and expressed by the Mie theory (Mie, 1908). This theory was particularly discussed by Van de Hulst (Van de Hulst, 1981) and also in part by many other authors (for example Aden, 1951; Deirmendjian et al., 1961; Wyatt, 1962; Kattawar & Plass, 1967; Dave, 1969; Hansen & Travis, 1974; and Liou, 1980). Here, we outline the basic equations of the Mie scattering behind the computation procedures.

1. Mie Scattering

Let λ represents the wavelength, r the radius of the sphere, x the Mie parameter ($x = 2\pi r/\lambda$), m the complex index of refraction ($m = n_r - in_i$), and θ the direction of scattered radiation measured from the forward direction. From Maxwell's equations, we can defined two complex functions $S_1(x,m,\theta)$ and $S_2(x,m,\theta)$ related to the amplitude of the scattered radiation, respectively, perpendicular and parallel to the plane of scattering:

$$S_1(x, m, \theta) = \sum_{n=1}^{\infty} \frac{(2n+1)}{n(n+1)} [a_n(x, m)\pi_n(\cos\theta) + b_n(x, m)\tau_n(\cos\theta)]$$

and

$$S_2(x, m, \theta) = \sum_{n=1}^{\infty} \frac{(2n+1)}{n(n+1)} [a_n(x, m)\tau_n(\cos\theta) + b_n(x, m)\pi_n(\cos\theta)].$$

1.1. Computation of $a_n(x,m)$ and $b_n(x,m)$

The complex functions $a_n(x,m)$ and $b_n(x,m)$ are given by

$$a_n(x, m) = \frac{\psi'_n(mx)\psi_n(x) - m\psi_n(mx)\psi'_n(x)}{\psi'_n(mx)\xi_n(x) - m\psi_n(mx)\xi'_n(x)}$$

and

$$b_n(x, m) = \frac{m\psi'_n(mx)\psi_n(x) - \psi_n(mx)\psi'_n(x)}{m\psi'_n(mx)\xi_n(x) - \psi_n(mx)\xi'_n(x)},$$

where the prime denotes derivative of the function with respect to the argument (x or mx), and $\psi_n(z = x \text{ or } mx)$ and $\xi_n(z = x)$ are the Ricatti-Bessel functions defined as

$$\psi_n(z) = \left(\frac{1}{2}\pi z\right)^{\frac{1}{2}} J_{n+\frac{1}{2}}(z) = zj_n(z),$$

$$\chi_n(z) = -\left(\frac{1}{2}\pi z\right)^{\frac{1}{2}} N_{n+\frac{1}{2}}(z) = -zn_n(z), \text{ and}$$

$$\xi_n(z) = \left(\frac{1}{2}\pi z\right)^{\frac{1}{2}} H_{n+\frac{1}{2}}^{(2)}(z) = zh_n^{(2)}(z) = \psi_n(z) + i\chi_n(z)$$

where $J_{n+\frac{1}{2}}$, $N_{n+\frac{1}{2}}$, and $H_{n+\frac{1}{2}}^{(2)}$ are the Bessel functions of the first, second, and third kind, respectively, and j_n , n_n , $h_n^{(2)}$ are the corresponding spherical Bessel functions. $N_{n+\frac{1}{2}}$ is also called the Neumann functions and $H_{n+\frac{1}{2}}^{(2)}$ the half integral order Hankel function of the second kind.

In order to make the computational work more convenient, it is useful to introduce the logarithmic derivative of the Ricatti-Bessel functions (*Infeld, 1947; Aden, 1951; Kattawar & Plass, 1967*):

$$D_n(z) = \frac{d}{dz} [\ln \psi_n(z)] \text{ and}$$

$$G_n(z) = \frac{d}{dz} [\ln \xi_n(z)].$$

Using these equations, $a_n(x,m)$ and $b_n(x,m)$ may be rewritten as

$$a_n(x, m) = \frac{\psi_n(x) D_n(mx) - mD_n(x)}{\xi_n(x) D_n(mx) - mG_n(x)}$$

and

$$b_n(x, m) = \frac{\psi_n(x) mD_n(mx) - D_n(x)}{\xi_n(x) mD_n(mx) - G_n(x)}.$$

Expressions of $a_n(x,m)$ and $b_n(x,m)$ are now reduced to a ratio of Ricatti-Bessel functions involving real arguments and a ratio of "D_n(mx or x) and G_n(x)" functions which are easily computable. Examples of $a_n(x,m)$ and $b_n(x,m)$ for $m=1.33-i 0.001$ and for $x=10$ and $x=50$ (which means respectively $r \approx 0.8 \mu\text{m}$ and $r \approx 4.0\mu\text{m}$ at $0.50 \mu\text{m}$) are shown in Fig. 1 and 2.

Also, in order to save time, we use in 6S the criterion defined by *Deirmendjian et al., 1961*:

"the quantities a_n and b_n are terminated either when $(a_n a_n^* + b_n b_n^*)/n < 10^{-14}$ "

1.1.1. Computation of the Ricatti-Bessel function.

The ratio of Ricatti-Bessel functions can be reduced to a ratio of spherical Bessel functions with

a real argument x as follows:

$$\frac{\Psi_n(x)}{\xi_n(x)} = \frac{j_n(x)}{h_n^{(2)}(x)} = \frac{j_n(x)}{j_n(x) - in_n(x)}$$

The spherical Bessel functions $j_n(x)$, $n_n(x)$ or $h_n^{(2)}(x)$ have different behaviors depending on if they are below or above the transition line defined by $x^2 = n(n+1)$. Below the transition line ($n(n+1) < x^2$), they behave as oscillating functions of both order and argument, whereas above the transition line ($n(n+1) > x^2$) their behavior becomes monotonic..

It has been shown by many authors that $n_n(x)$ or $h_n^{(2)}(x)$ can be processed using an upward recurrence (for any values of n and x). Functions $n_n(x)$ are computed using

$$n_{n+1}(x) = \frac{2n+1}{x} n_n(x) + n_{n-1}(x)$$

with

$$n_0(x) = -\frac{\cos(x)}{x} \quad n_1(x) = -\frac{\cos(x)}{x^2} - \frac{\sin(x)}{x}$$

Figure 3 show examples of the $n_n(x)$ function for $x=10$ and $x=50$.

For $j_n(x)$, we use a similar recurrence

$$j_{n+1}(x) = \frac{2n+1}{x} j_n(x) + j_{n-1}(x)$$

but, as it is explained in *Corbató & Uretsky's* paper (1959), the function $j_n(x)$ cannot be computed by an upward recurrence "since upward recursion (except in the region of the x - n plane where j oscillate) would bring about a rapid loss of accuracy". Then, a downward recurrence is called for, but we have to define the starting value of n , and for that purpose we use *Corbato & Uretsky's* work which is summarized hereafter. Let N be the starting order of the recursion with $N(N+1) > x^2$. In their paper, they show "that rather than accurately evaluate $j_N(x)$ and $j_{N-1}(x)$ to start the process, a very approximately starting the recursion at a higher order will give a set of numbers which are accurately proportional to the j_n over the desired range of n from 0 to N ". Let \bar{j}_n be one of these numbers.

They propose to define the higher order v by

$$v = N' - \frac{\ln \varepsilon_N}{\ln 2} \left[A + \frac{Bu'(2-u'^2)}{2(1-u'^2)} \right]$$

where

$A = 0.10$ and $B = 0.35$,

$\varepsilon_N = 2^{-30}$ (this value comes from the fact that computers can generally store floating point numbers with a 30 binary digit mantissa), and

$u' = 2x / (2N'+1)$ with $N' = N$ or $N' = x - \frac{1}{2} + \sqrt{-\frac{\ln \varepsilon_N}{\ln 2} Bx}$ such that v be the lower, with however $N' \geq N$.

To avoid computational difficulties above the transition line, *Corbato & Uretsky* worked with the ratio $\bar{r}_n = \bar{j}_{n+1} / \bar{j}_n$ using the recurrence relation

$$\bar{r}_{n-1} = \frac{x}{2n+1-x\bar{r}_n}$$

with the starting condition $\bar{r}_v = 0$. The recursion is continued downward until a ratio \bar{r}_n which exceeds the unity is reached. Then, they set $\bar{j}_{n+1} = \bar{r}_n$ and $\bar{j}_n = 1$, and continue downward using the recurrence relation

$$\bar{j}_{n-1}(x) = \frac{2n+1}{x} \bar{j}_n(x) + \bar{j}_{n+1}(x).$$

The positive number \bar{j}_n is defined by $\bar{j}_n(x) = \alpha j_n(x)$ with a constant of proportionality α obtained from the relation

$$\alpha = (\bar{j}_0(x) - x\bar{j}_1(x)) \cos(x) + x\bar{j}_0(x) \sin(x).$$

Figure 3 also show examples of the $j_n(x)$ function for $x=10$ and $x=50$.

1.1.2. Computation of the $D_n(mx \text{ or } x)$ and $G_n(x)$ functions

As *Kattawar & Plass* (1967) pointed out, the procedure for computing $D_n(z)$ by an upward recurrence is unstable, then a downward process is needed, and $D_n(z)$ is defined using

$$D_{n-1}(z) = n/z - \frac{1}{D_n(z) + n/z}.$$

Calculations have to be started at an order $n = v' \gg |z|$ with a starting value which is not really important because the series converges rapidly to the exact value (then $D_{v'}(z) = 0$ is a convenient value). When $n < |z|$, $D_n(z)$ becomes oscillatory, and then there is no problem for the calculation using the recurrence relation. For practical reasons, we selected in 6S $v' = v$ as defined for j_n .

Kattawar & Plass also showed that $G_n(x)$ may always be calculated using an upward process with a starting value $G_0(x) = -i$:

$$G_n(x) = -n/x - \frac{1}{G_{n-1}(x) - n/x}$$

Figure 4 illustrates examples of the $D_n(x)$ function, Fig. 5 - the $D_n(mx)$ function, and Fig. 6 the $G_n(x)$ function.

1.2. Computation of $\pi_n(\cos\theta)$ and $\tau_n(\cos\theta)$

Functions π_n and τ_n depend only on the scattering angle θ . They are related to the associated Legendre polynomials $P_n^1(\cos\theta)$:

$$\pi_n(\cos\theta) = \frac{1}{\sin\theta} P_n^1(\cos\theta)$$

$$\tau_n(\cos\theta) = \frac{d}{d\theta} P_n^1(\cos\theta)$$

and are computed from upward recurrence relations defined as

$$n\pi_{n+1}(\cos\theta) = (2n+1)\cos\theta\pi_n(\cos\theta) - (n+1)\pi_{n-1}(\cos\theta)$$

$$\tau_{n+1}(\cos\theta) = (n+1)\cos\theta\pi_{n+1}(\cos\theta) - (n+2)\pi_n(\cos\theta)$$

with the starting values $\pi_0(\cos\theta) = 0$ and $\pi_1(\cos\theta) = 1$.

Examples of functions π_n and τ_n are shown Fig. 7 for $n=1$ to 6 and for $0^\circ < \theta < 90^\circ$.

2. Computation of the physical properties of a particle (see for example Liou, 1980)

2.1. Extinction

The **extinction cross section** σ_e , which denotes the amount of energy removed (scattered and absorbed) from the original beam by the particle, is obtained considering a point in the forward direction ($\theta=0$) in the "far field". If we consider an isotropic homogeneous sphere, the extinction cross section is given by

$$\sigma_e(\lambda, r, m) = \frac{4\pi}{(2\pi/\lambda)^2} \Re_e[S(x, m, \theta = 0)]$$

with

$$S(x, m, \theta = 0) = S_1(x, m, \theta = 0) = S_2(x, m, \theta = 0) = \frac{1}{2} \sum_{n=1}^{\infty} (2n+1)[a_n(x, m) + b_n(x, m)].$$

Thus the **extinction efficiency** Q_e is defined by

$$Q_e(\lambda, r, m) = \frac{\sigma_e(\lambda, r, m)}{\pi r^2} = \frac{2}{x^2} \sum_{n=1}^{\infty} (2n+1) \Re_e[a_n(x, m) + b_n(x, m)].$$

2.2. Scattering

The **scattering cross section** σ_s is derived by a similar way, but considering a scattered light in an arbitrary direction, by

$$\sigma_s(\lambda, r, m) = \frac{\pi}{(x/r)^2} \int_0^\pi [S_1(x, m, \theta) S_1^*(x, m, \theta) + S_2(x, m, \theta) S_2^*(x, m, \theta)] \sin \theta \, d\theta .$$

Owing to the functions π_n and τ_n , we have to integrate products of the associated Legendre polynomials. Using the orthogonal and recurrence properties of these polynomials, the scattering cross section can be written

$$\sigma_s(\lambda, r, m) = \frac{2\pi}{(x/r)^2} \sum_{n=1}^{\infty} (2n+1) [a_n(x, m) a_n^*(x, m) + b_n(x, m) b_n^*(x, m)],$$

where the asterisk denotes the complex conjugate value, and the **scattering efficiency** Q_s can be evaluated by the relation

$$Q_s(\lambda, r, m) = \frac{\sigma_s(\lambda, r, m)}{\pi r^2} = \frac{2}{x^2} \sum_{n=1}^{\infty} (2n+1) [a_n(x, m) a_n^*(x, m) + b_n(x, m) b_n^*(x, m)]$$

2.3. Absorption

The **absorption cross section** σ_a and the **absorption efficiency** Q_a can be deduced as

$$\sigma_a(\lambda, r, m) = \sigma_e(\lambda, r, m) - \sigma_s(\lambda, r, m) \text{ and}$$

$$Q_a(\lambda, r, m) = Q_e(\lambda, r, m) - Q_s(\lambda, r, m) .$$

2.4. Phase function

On the basis of the Stokes parameters, the intensity I of the electromagnetic waves at each point and in any given direction can be related to the incident intensity [formula]

$$I = M_{11} I_0$$

with

$$M_{11}(\lambda, r, m, \theta) = \frac{1}{2x^2} [S_1(x, m, \theta) S_1^*(x, m, \theta) + S_2(x, m, \theta) S_2^*(x, m, \theta)].$$

The angular distribution of the scattered energy for a single sphere (also called **Phase function**) $P_{11}(\lambda, r, m, \theta)$ can be defined by

$$M_{11}(\lambda, r, m, \theta) = \frac{\sigma_s(\lambda, r, m)}{4\pi r^2} P_{11}(\lambda, r, m, \theta) .$$

Then

$$P_{11}(\lambda, r, m, \theta) = \frac{2\pi}{(x/r)^2 \sigma_s(\lambda, r, m, \theta)} \left[S_1(x, m, \theta) S_1^*(x, m, \theta) + S_2(x, m, \theta) S_2^*(x, m, \theta) \right].$$

It can be checked that

$$\int_0^{2\pi} \int_0^{\pi} P_{11}(\lambda, r, m, \theta) \sin \theta \, d\theta \, d\phi = 4\pi.$$

3. Physical properties of a sample of identical particles

We now consider a sample of identical particles whose size is described by the **size distribution** $n(r)$ (in $\text{cm}^{-3} \mu\text{m}^{-1}$) such that

$$\int_0^{\infty} n(r) \, dr = \int_0^{\infty} \frac{dN(r)}{dr} \, dr = 1,$$

where $dN(r)$ represents the number of particle per unit volume having a radius between r and $r+dr$.

In 6S, we selected several possibilities to represent the size distribution, thus the user will be allowed to choose between 4 options:

1 - Junge Power-Law function. *Junge* (1952) showed that the size distribution of aerosols whose radii are larger than $0.1 \mu\text{m}$ may be described by

$$\frac{dN(r)}{d \log r} = \ln(10) c r_0^\alpha \left(\frac{1}{r} \right)^{\alpha-1} \quad \text{or} \quad \frac{dN(r)}{dr} = c r_0^\alpha \left(\frac{1}{r} \right)^\alpha$$

where α varies between 3 and 5, c is the number density of particles with radius r_0 , and r_0 is an arbitrary radius. Figure 8-a shows an example of Junge Power-Law function which is the "Model C" defined by *Deirmendjian* (1969), for $c \cdot r_0^\alpha = 1$ and $\alpha = 4$

2 – Modified Gamma distribution function. Used by *Deirmendjian* (1964) to compute scattering properties of water clouds and haze and to fit aerosol measurements. Also employed by Mie in the Mie and diffraction calculations.

$$\frac{dN(r)}{dr} = A(r/r_0)^\alpha \exp(-b(r/r_0)^\gamma) \quad \text{with} \quad r_0 = 1 \mu\text{m}$$

An example of Modified Gamma distribution function is given Fig. 8-b (Volcanic Ash defined in WCP 112, $A=5461.33$, $\alpha = 1.0$, $\gamma = 0.5$, $b = 16$).

3 - Log-Normal distribution function. Based on the Junge Power-Law function, *Davies* (1974) introduced this function to take into account large particles:

$$\frac{dN(r)}{d \log r} = \frac{N}{\sqrt{2\pi} \log \sigma} \exp\left(-\frac{1}{2} \left(\frac{\log r - \log r_M}{\log \sigma}\right)^2\right)$$

where r_M is the mean radius of particles, and σ the standard deviation of r .

Figure 8-c illustrates examples of Log-Normal distribution functions which are the 3 three components of the "Continental Model" defined in WCP 112 (see subroutine AEROSO to find r_M and σ).

4 - Sun photometer measurements. You enter directly $dV(r)/d\log r \approx r^4 dN(r)/dr$.

Figure 9 shows the same function than Fig. 8 but for $dV(r)/d\log(r)$.

Under the assumption of "independent scattering", which means that particles are sufficiently far from each other compared to the incident wavelength to consider just one scattering, it is possible to add scattered intensities independently of the phase of the wave. Then we can define the radiative characteristics upon the particle size distribution by

- The **extinction** (e), **scattering** (s) and **absorption** (a) coefficient

$$k_{e,s,a}(\lambda, m) = \int_{r_{\text{mix}}}^{r_{\text{max}}} Q_{e,s,a}(\lambda, r, m) \pi r^2 \frac{dN(r)}{dr} dr ;$$

- The **normalized phase function**

$$P(\lambda, m, \theta) = \frac{1}{k_s(\lambda, m)} \int_{r_{\text{mix}}}^{r_{\text{max}}} M_{11}(\lambda, r, m, \theta) 4\pi r^2 \frac{dN(r)}{dr} dr ;$$

- We now introduce the **single scattering albedo** ω_0 which represents the percentage of energy removed from the incident beam which will reappear as single scattered radiation:

$$\omega_0(\lambda, m) = \frac{k_s(\lambda, m)}{k_e(\lambda, m)} .$$

Computationally, $k_{e,s,a}(\lambda, m)$ and $P(\lambda, m, \theta)$ are integrated step by step following:

$$k_{e,s,a}(\lambda, m) = \sum_{r_{\text{min}}}^{r_{\text{max}}} Q_{e,s,a}(\lambda, r, m) \pi r^2 \frac{dN(r)}{dr} \Delta r$$

and

$$P(\lambda, m, \theta) = \frac{1}{k_s(\lambda, m)} \sum_{r_{\text{min}}}^{r_{\text{max}}} M_{11}(\lambda, r, m, \theta) 4\pi r^2 \frac{dN(r)}{dr} \Delta r ,$$

where Δr is defined by

$$\log\left(\frac{r + \Delta r}{r}\right) = 0.03.$$

The value 0.03 was selected to preserve a good accuracy with a reasonable computational time. For example, *D'Almeida* used a very small step width, 0.011, for the computations given in his book (*D'Almeida et al.*, 1991). The logarithmic expression of Δr comes from the fact that size distributions can be frequently described by a logarithmic shape (*Junge*, 1952; *Davies*, 1974).

Finally, in order to save computational time, we defined a criterion on the summation such that the computations are not performed either when

$$\left(\frac{n_i}{n} \pi r^2 \frac{dN(r)}{dr} \Delta r\right) \frac{1}{\sqrt{\lambda}} < 10^{-8}$$

where n_i/n is the percentage density of particles (see subroutine AEROSO for some examples). The latter criterion has been tested between 0.4 and 4.0 μm .

4. Physical properties of a mixture of aerosol types

We now consider a mixture of particles originating from different sources (4 max.). The mixing is treated in the same way that the one used to generate the database in the AEROSO subroutine.

Let us recall that the mixture of individual components (or type) of an aerosol is characterized by the percentage density of particles n_i/n , and if we assume that the particles are spherical, each type i is described by its size distribution (then by its microphysical identity: r_{Mi} and σ_i , see Table 1 for some examples (*Shettle and Fenn*, 1976; *World Climate Programme*, 1986), and by its complex refractive index m_i (see Table 2, from *Shettle & Fenn*, 1976, 1979; *World Climate Programme*, 1986; *D'Almeida et al.*, 1991). For the size distribution, the Log-Normal distribution is well adapted to emphasize the individual components of a mixture (*Davies*, 1974, *D'Almeida et al.*, 1991).

5. Examples and comparisons

The comparison of the computed K_e , K_s and ω_0 values, normalized at 550 nm, obtained by 6S with those given by *World Climate Programme* (1986) are reported for a Continental and an Urban dry aerosol model respectively in Table 3 and Table 4. The asymmetry parameter g is also reported in this table. In 6S, this parameter is already computed in an another subroutine, but

we can compute it here using

$$g = \frac{\int_{-1}^{+1} \cos \theta P(\lambda, m, \theta) d \cos \theta}{\int_{-1}^{+1} P(\lambda, m, \theta) d \cos \theta}$$

The comparison of the phase function of a Continental model (*WMO/WCP-112*) computed by the MIE subroutine with those by a precise code (subroutine AEROSO) is reported Fig.10 for several wavelengths. Also, in Fig. 11 we show the phase function computed using the volumic distribution $dV/d\log r$ provided by a CIMEL sunphotometer during the SCAR-A field experiment (Sulfate Clouds Aerosol and Reflectances - America) that took place in July 1993 in the Eastern USA.

Parameters:

For IAER=8 (Multimodal Log-Normal (up to 4 modes))

r_{\min} , r_{\max} , icp

then for $k=1$ to icp, enter:

σ , r_M , C_{ij}

$r_n(\lambda_j)$, $j=1,20$

$r_i(\lambda_j)$, $j=1,20$

where r_{\min} and r_{\max} are the radii min and max of the aerosol,

icp is the number of mode (component),

σ and r_M are parameters of the Log-Normal size distributions,

C_{ij} is the percentage density of particles (see subroutine AEROSO),

r_n and r_i are the real and imaginary index of refraction of each component,

with $r = r_n - i \cdot r_i$. You have to enter these parameters for 20 wavelengths used to compute the atmospheric signal, which are:

0.350, 0.400, 0.412, 0.443, 0.470, 0.488, 0.515, 0.550, 0.590, 0.633, 0.670, 0.694, 0.760, 0.860, 1.240, 1.536, 1.650, 1.950, 2.250, 3.750

For IAER=9 (Modified Gamma distribution)

r_{\min} , r_{\max}

α , b , γ

$r_n(\lambda_j)$, $j=1,20$

$r_i(\lambda_j)$, $j=1,20$

where α , b , and γ are the parameters of the Modified Gamma size distribution.

For IAER=10 (Junge Power-Law distribution)

r_{\min} , r_{\max}

α

$r_n(\lambda_j)$, $j=1,20$

$r_i(\lambda_j)$, $j=1,20$

where α is the parameter of the Junge Power-Law size distribution.

For IAER=11 (Sun-photometer distribution (50 values max))

irsunph

for $k=1$ to irsunph enter:

r and $dV/d\log r$

$r_n(\lambda_j)$, $j=1,20$

$r_i(\lambda_j)$, $j=1,20$

where irsunph is the number of value and $dV/d\log r$ is usually provided by sunphotometers.

Table 1. Microphysical characteristics of the aerosol type (dry particles) used for the comparisons shown in Tables 3 and 4 (from WMO-WCP112).

	Dust-Like	Water Soluble	Oceanic	Soot
$r_{Mi}(\mu\text{m})$	0.500	0.0050	0.30	0.0118
σ_i	2.990	2.990	2.51	2.00

Table 2. Complex refractive indexes of the aerosol types (dry particles) used for the comparisons shown in Tables 3 and 4 (from WMO-WCP112).

λ (μm)	Dust-Like		Water Soluble		Oceanic		Soot	
	n_r	n_i	n_r	n_i	n_r	n_i	n_r	n_i
0.400	1.530	8.00E-3	1.530	5.00E-3	1.385	9.90E-9	1.750	0.460
0.488	1.530	8.00E-3	1.530	5.00E-3	1.382	6.41E-9	1.750	0.450
0.515	1.530	8.00E-3	1.530	5.00E-3	1.381	3.70E-9	1.750	0.450
0.550	1.530	8.00E-3	1.530	6.00E-3	1.381	4.26E-9	1.750	0.440
0.633	1.530	8.00E-3	1.530	6.00E-3	1.377	1.62E-8	1.750	0.430
0.694	1.530	8.00E-3	1.530	7.00E-3	1.376	5.04E-8	1.750	0.430
0.860	1.520	8.00E-3	1.520	1.20E-2	1.372	1.09E-6	1.750	0.430
1.536	1.400	8.00E-3	1.510	2.30E-2	1.359	2.43E-4	1.770	0.460
2.250	1.220	9.00E-3	1.420	1.00E-2	1.334	8.50E-4	1.810	0.500
3.750	1.270	1.10E-2	1.452	4.00E-3	1.398	2.90E-3	1.900	0.570

Table 3. Comparison between 6S and WMO-WCP112 for the Continental model (normalized value-dry particles).

λ (μm)	K_{ext}		K_{sca}		ω_0		g	
	6S	WMO	6S	WMO	6S	WMO	6S	WMO
0.400	1.40	1.40	1.27	1.27	0.902	0.901	0.643	0.646
0.488	1.14	1.14	1.03	1.03	0.900	0.898	0.637	0.640
0.515	1.08	1.08	0.967	0.967	0.899	0.897	0.635	0.638
0.550	1.00	1.00	0.893	0.891	0.893	0.891	0.634	0.637
0.633	0.849	0.849	0.755	0.754	0.890	0.888	0.629	0.633
0.694	0.760	0.760	0.671	0.669	0.881	0.879	0.628	0.631
0.860	0.577	0.577	0.487	0.486	0.844	0.841	0.629	0.633
1.536	0.282	0.283	0.212	0.212	0.753	0.750	0.641	0.645
2.250	0.150	0.151	0.115	0.115	0.765	0.761	0.738	0.741
3.750	0.101	0.103	0.0796	0.0805	0.790	0.785	0.777	0.779

Table 4. Comparison between 6S and WMO-WCP112 for the Urban model (normalized value-dry particles).

λ (μm)	K_{ext}		K_{sca}		ω_0		g	
	6S	WMO	6S	WMO	6S	WMO	6S	WMO
0.400	1.48	1.48	0.980	0.976	0.664	0.660	0.600	0.600
0.488	1.16	1.17	0.766	0.762	0.658	0.654	0.594	0.593
0.515	1.09	1.09	0.715	0.711	0.655	0.651	0.592	0.592
0.550	1.00	1.00	0.651	0.647	0.651	0.647	0.591	0.591
0.633	0.828	0.829	0.535	0.532	0.646	0.641	0.587	0.587
0.694	0.733	0.733	0.466	0.462	0.635	0.631	0.585	0.585
0.860	0.542	0.542	0.322	0.319	0.593	0.588	0.584	0.583
1.536	0.242	0.243	0.111	0.111	0.460	0.455	0.564	0.565
2.250	0.123	0.124	0.0428	0.0426	0.347	0.342	0.583	0.585
3.750	0.0647	0.0659	0.0177	0.0181	0.274	0.274	0.579	0.587

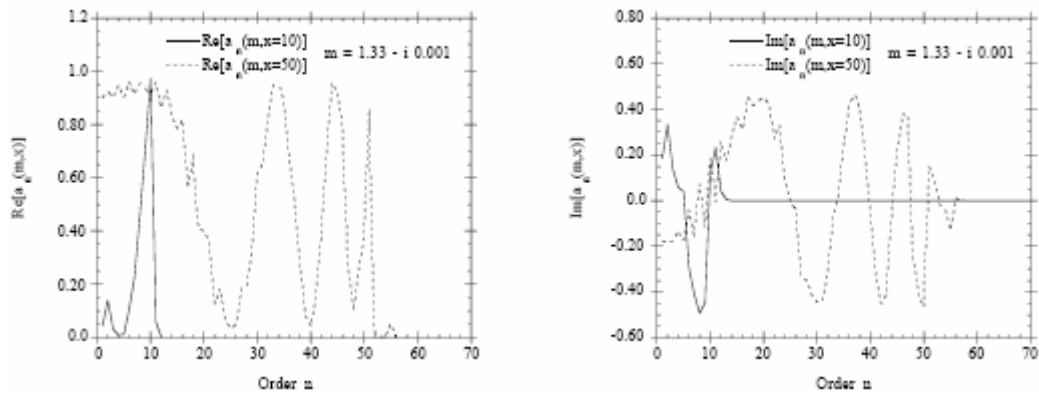


Fig. 1. Examples of an $a_n(m,x)$ function.

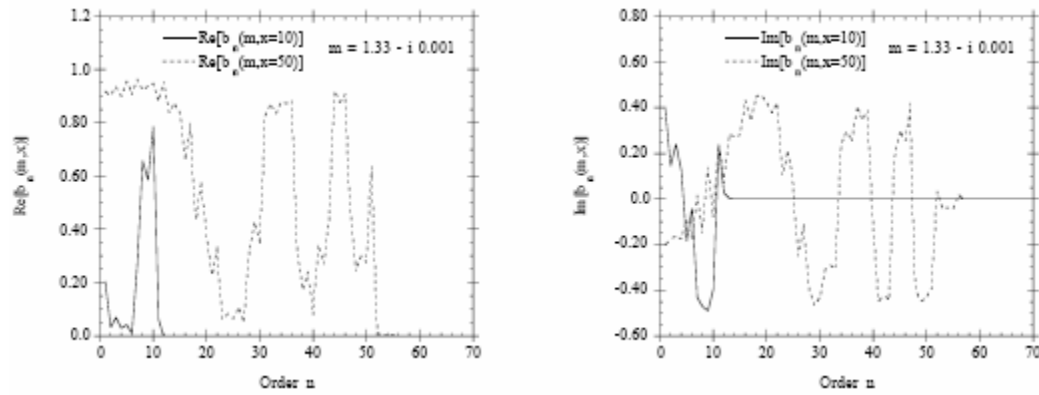


Fig. 2. Examples of a $b_n(m,x)$ function.

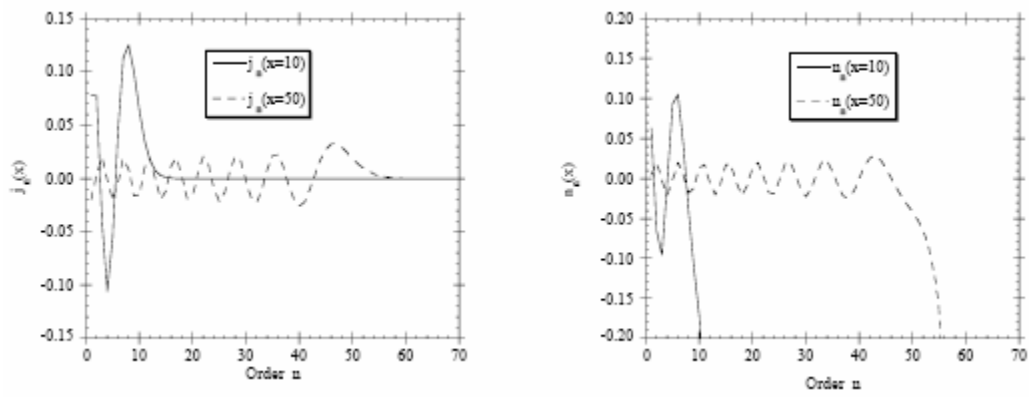


Fig. 3. Examples of spherical Bessel functions $j_n(x)$ and $n_n(x)$.

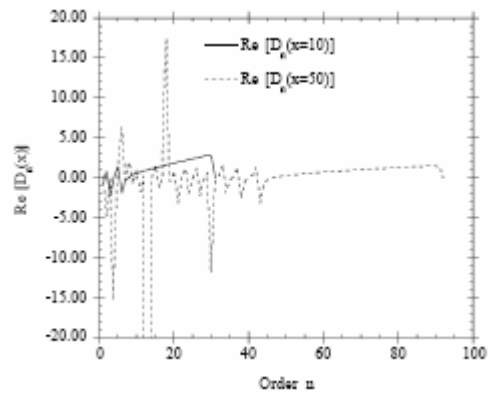


Fig. 4. Example of a $D_n(x)$ function.

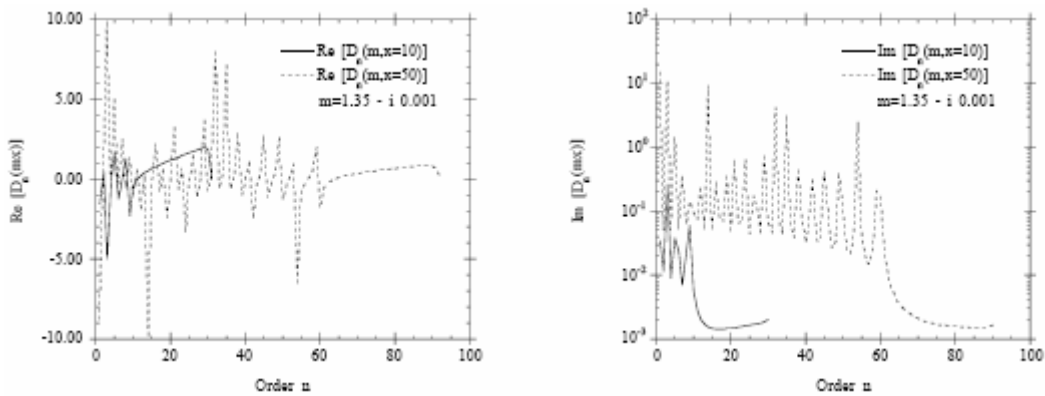


Fig. 5. Examples of a $D_n(m,x)$ function.

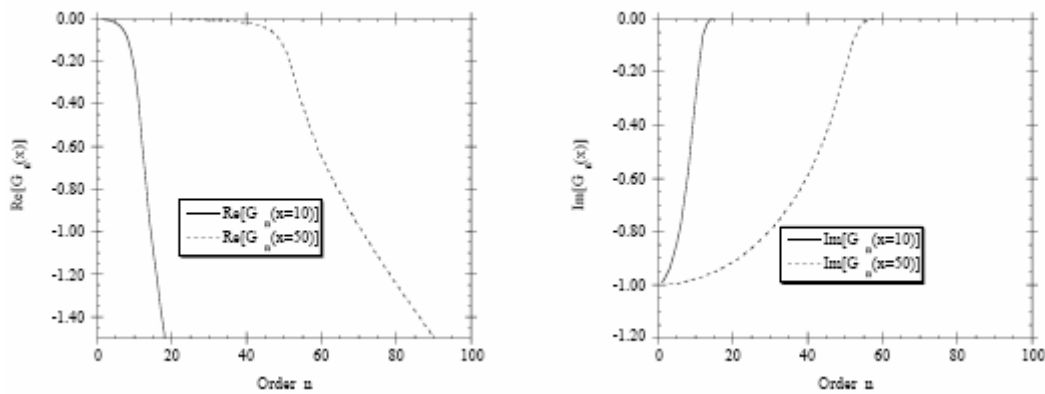


Fig. 6. Examples of a $G_n(x)$ function.

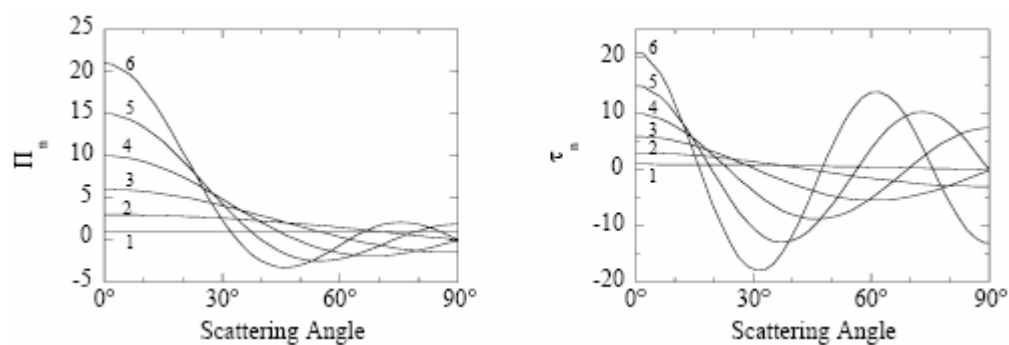


Fig. 7. Examples of functions $\pi_n(\theta)$ and $\tau_n(\theta)$ for $n=1$ to 6.

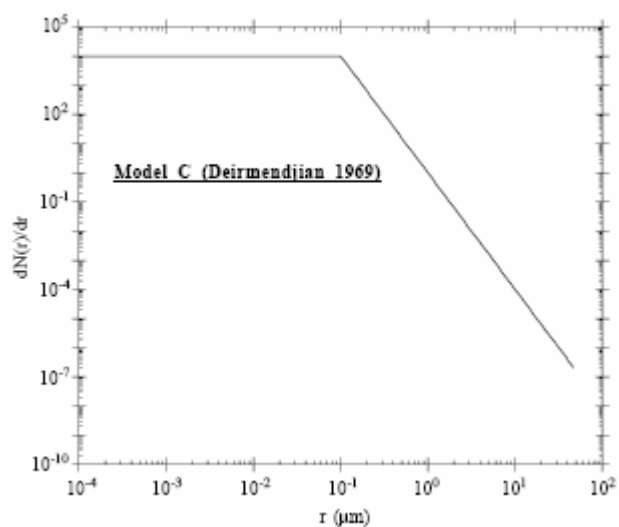


Fig. 8a. Junge Power-Law distribution: Model C (*Deirmendjian, 1969*).

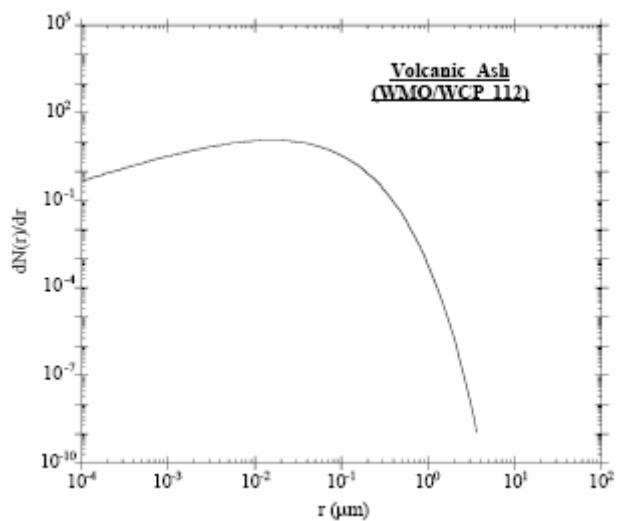


Fig. 8b. Modified Gamma distribution function: Volcanic Ash (*WCP 112*).

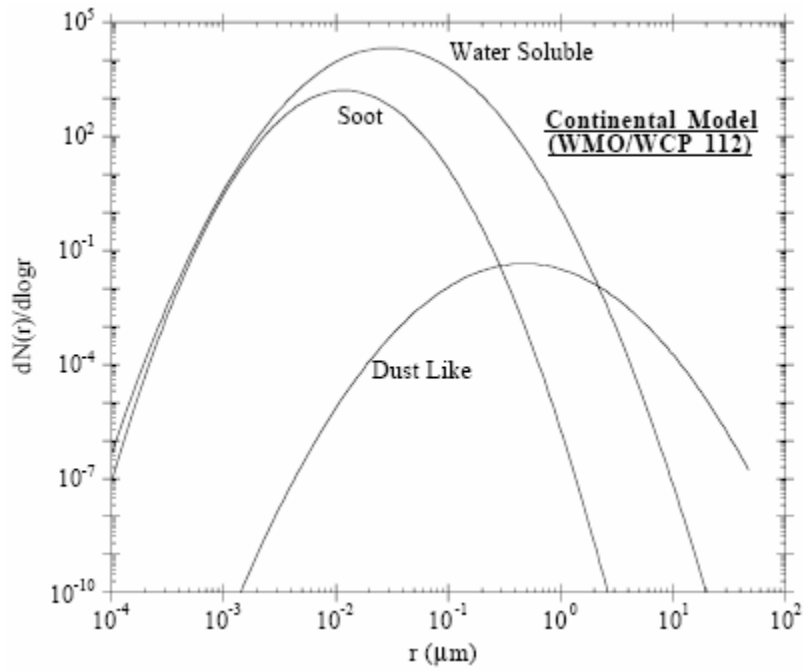


Fig. 8c. Log-Normal distribution function: Continental model (WCP 112).

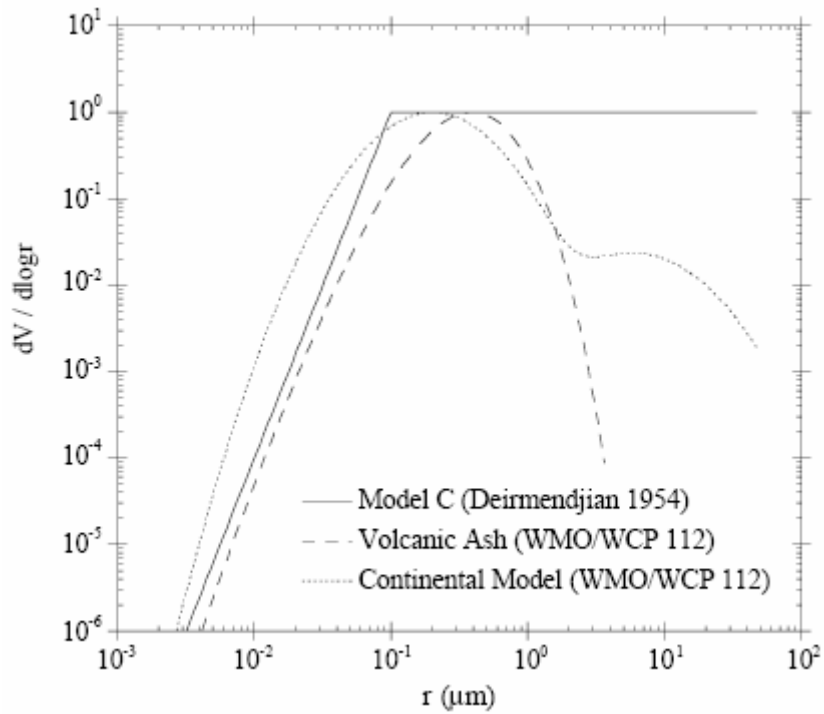


Fig. 9. Same as Fig. 8 but represented for $dV/d\log r$.

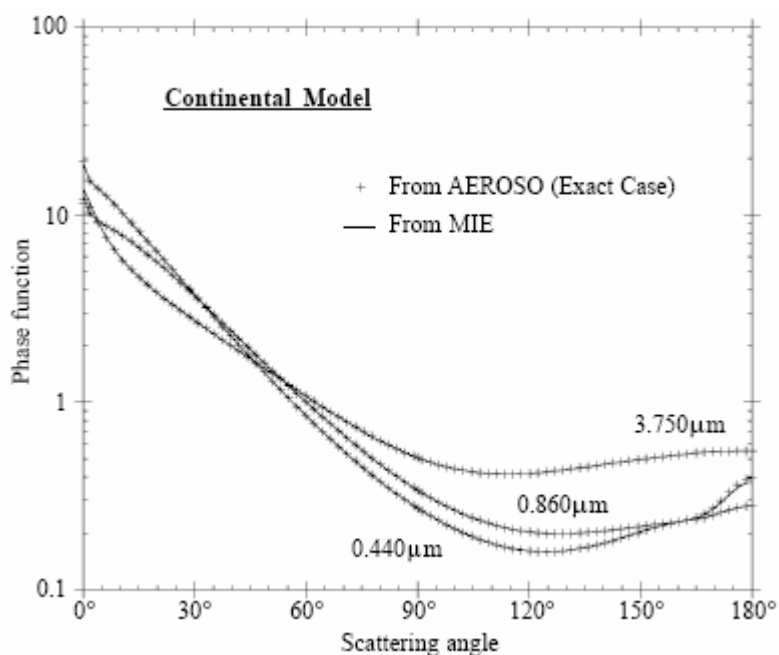


Fig. 10. Phase function (dry particle) as computed by the MIE subroutine and the one generated by the AEROSO subroutine (exact case).

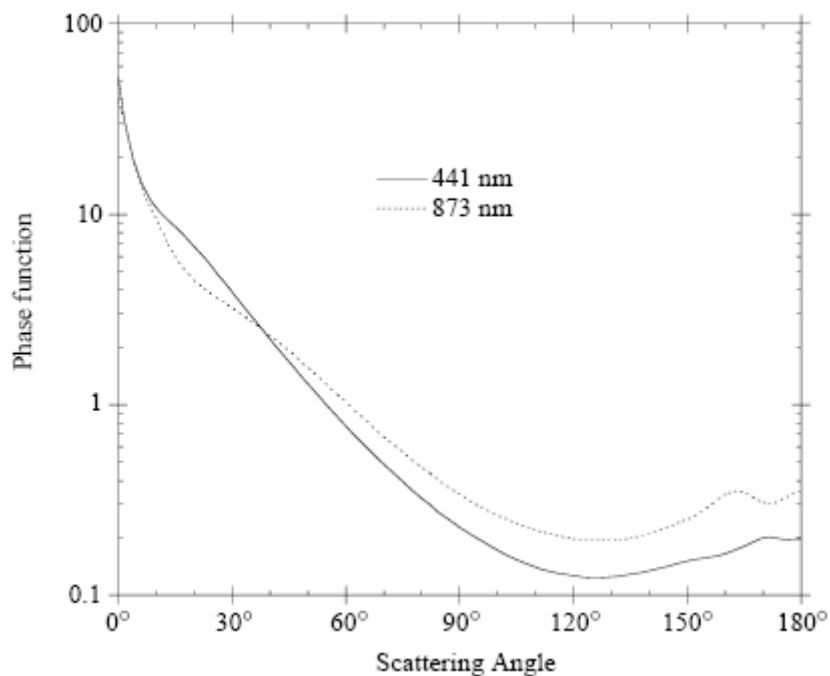


Fig. 11. Phase function as computed by the MIE subroutine using $dV/d\log r$ provided by a sunphotometer CIMEL during the SCAR-A experiment (Hog Island, July 11, 1993).

References:

- A.L. Aden, Electromagnetic scattering from spheres with sizes comparable to the wavelength, *Journal of Applied Physics*, 22(5), 601-605, 1951.
- F.J. Corbato and J.L. Uretsky, Generation of spherical Bessel functions in digital computers, *Journal of the Association of Computing Machinery*, 6, 366-375, 1959.
- G.A. D'Almeida, P. Koepke, and E.P. Shettle, Atmospheric aerosols global climatology and radiative characteristics, A. Deepak Publishing, Hampton, 1991.
- J.V. Dave, Scattering of visible light by large water spheres, *Applied Optics*, 8(1), 155-164, 1969.
- C.N. Davies, Size distribution of atmospheric particles, *Journal of Aerosol Science*, 5, 293-300, 1974.
- D. Deirmendjian, Scattering and polarization properties of water clouds and hazes in the visible and infrared, *Applied Optics*, 3, 187-196, 1964.
- D. Deirmendjian, R. Clasen, and W. Viezee, Mie scattering with complex index of refraction. *Journal of the Optical Society of America*, 51(6), 620-633, 1961.
- D. Deirmendjian, Electromagnetic scattering on spherical polydispersion, American Elsevier Pub. Co. New-York, 1969.
- J.E. Hansen and L. Travis, Light scattering in planetary atmospheres, *Space Science Reviews*, 16, 527-610, 1974.
- L. Infeld, The influence of the width of the gap upon the theory of antennas, *Quarterly of Applied Mathematics*, 5(2), 113-132, 1947.
- C.E. Junge, Gesetzmäßigkeiten in der droßenverteilung atmosphärischer aerosole über dem kontinent, *Beitraege der Deirsch Wetterdienst U.S.-Zone*, 35, 261-277, 1952.
- G.W. Kattawar and G.N. Plass, Electromagnetic scattering from absorbing spheres, *Applied Optics*, 6(8) 1377-1382, 1967.
- K.N. Liou, An introduction to atmospheric radiation, Academic Press Inc., San Diego, 1980.
- G. Mie, Beigrade zur Optik trüber medien, speziell kolloidaler metallösungen, *Annalen der Physik*, 25, 377 - 445, 1908.
- E.P. Shettle and R.W. Fenn, Models of atmospheric aerosols and their optical properties, in: *Optical Propagation in the Atmosphere*, AGARD-Cp-183, NTIS, ADA 028615, 1976.
- E.P. Shettle and R.W. Fenn, Models for the aerosol of the lower atmosphere and the effect of humidity variations on their optical properties, AFGL-TR-79-0214, *Environmental Research*

Paper, No 675, NTIS, ADA 085951, 1979.

H.C. Van De Hulst, *Light scattering by small particles*, Dover Publications, New York, Dover, 1981.

World Climate Programme, WCP-55, Report of the expert meeting on aerosols and their climatic effects (Eds. A. Deepak and H.E. Gerber), World Meteorological Organization, Geneva, 1983.

World Climate Programme, WCP-112, A preliminary cloudless standard atmosphere for radiation computation, World Meteorological Organization, WMO/TD-No 24, Geneva, 1986.

P.J. Wyatt, Scattering of electromagnetic plane waves from inhomogeneous spherically symmetric objects, *Physical Review*, 127(5), 1837-1843, 1962.

SUBROUTINE ODA550

Function: To compute the extinction cross section and the aerosol optical depth at $\lambda = 550$ nm from the vertical distributions of the particle density (in particules/cm³).

Description: We have considered the two profiles, suggested by *Mc Clatchey et al* (1971), corresponding to a visibility of 23 (clear) and 5 km (hazy) at ground level. The total numbers of aerosols for the clear atmosphere have been adjusted so that the total extinction coefficient at $\lambda = 550$ nm becomes identical to the values used by *Elterman* (1964).

This total extinction coefficient K (in km⁻¹) is obtained from

$$K^{550}(z) = \sigma_{550} 10^{-3} N(z),$$

where s is the extinction cross section in mm² and $N(z)$ the particle density (in part/cm³) (the factor 10^{-3} is to obtain an extinction coefficient in km⁻¹). σ was computed with the same aerosol model as the one defined by *Mc Clatchey et al.*, index of refraction equal to 1.50 and size distribution similar to *Deirmendjian's* model "C" (1969) (cut off has been extended from 5 to 10 μ m). The computed value of σ_{550} is 0.056032.

The optical thickness τ is defined by

$$\tau_{550} = \int_0^{+\infty} K^{550}(z) dz$$

We obtain the optical thicknesses at 550 nm, 0.235 and 0.780 respectively for the two standard visibilities 23 and 5 km. For another visibility, we compute a new profile particle density from those defined for 23 and 5 km. The calculations were made using the following interpolation:

$$N(z) = \frac{a(z)}{VIS} + b(z).$$

For example, we obtain:

$$\begin{aligned} \tau &= 0.152 && \text{for } V = 50 \text{ km,} \\ \tau &= 0.520 && \text{for } V = 8 \text{ km.} \end{aligned}$$

References:

R.A. Mc Clatchey, R.W. Fenn, J.E.A. Selby, F.E. Volz, and J.S. Garing. Optical properties of the atmosphere, AFCRL-TR-71-0279, *Environmental Research Paper*, No. 354, L.G. Hancom Fiel Bedford, Massachusetts, U.S.A., 1971.

- D. Deirmendjian, Electromagnetic scattering on spherical polydispersions, American Elsevier Pub. Co., New York, 290p. 1969.
- L. Elterman, Rayleigh and extinction coefficients to 50 km for the region 0.27 μm to 0.55 μm , *Applied Optics*, 3, 1139-1147, 1964.

SUBROUTINE ODRAYL

Function: To compute the molecular optical depth as a function of wavelength for any atmosphere defined by pressure and temperature profiles.

Description: The optical depth is written

$$\tau_{\lambda}^R = \int_0^{+\infty} \beta_{\lambda}(z) dz$$

where $\beta_{\lambda}(z)$ is the molecular extinction coefficient at altitude z and for wavelength λ . It can be obtained from

$$\beta_{\lambda}(z) = \sigma_{\lambda} N_r(z) 10^5,$$

with $N_r(z)$ is the molecules number/cm³ at altitude z , and σ_{λ} is the extinction (or scattering) cross section in cm².

These two quantities are defined by

$$\sigma_{\lambda} = \frac{24\pi^3 (n_s^2 - 1)^2}{\lambda^4 N_s^2 (n_s^2 + 2)^2} \left(\frac{6 + 3\delta}{6 - 7\delta} \right)$$

and

$$N_r(z) = N_s \frac{P(z)}{1013.25} \left(\frac{273.15 + 15}{T(z)} \right),$$

where $P(z)$ and $T(z)$ are respectively the pressure and temperature at the altitude z . Recall that n_s is the air refractive index calculated at 15°C and 1013 mb, N_s is the molecular density at $z = 0$ in STP conditions, and δ is the molecular depolarization factor.

We have taken:

* for refractive index

$$(n_s - 1) \cdot 10^8 = 8342.13 + \frac{2406030}{130 - \lambda^{-2}} + \frac{15997}{38.9 - \lambda^{-2}}$$

where λ is the frequency in cm⁻¹,

* $N_s = 2.54743 \cdot 10^{19}$,

* and the depolarization factor $\delta = 0.0279$ following *Young's* (1980).

This depolarization factor is also used to compute the Rayleigh phase function (see subroutine CHAND) according to

$$P(\Theta) = \frac{3}{4} \frac{1-\gamma}{1+2\gamma} (1 + \cos^2 \Theta) + \frac{3\gamma}{1+2\gamma},$$

where Θ is the scattering angle, and $\gamma = \delta / (2 - \delta)$.

References :

- B. Edlen, The refractive index of air, *Metrologia*, 2, 71-80, 1966.
- L. Elterman, Rayleigh and extinction coefficients to 50 km for the region 0.27 μm to 0.55 μm , *Applied Optics*, 3, 1139-1147, 1964.
- D.V. Hoyt, A redetermination of the Rayleigh optical depth and its application to selected solar radiation problems, *Journal of Applied Meteorology*, 16, 432 - 436, 1977.
- A. T. Young, Revised depolarization corrections for atmospheric extinction, *Applied Optics*, 19, 3427-3428, 1980.

SUBROUTINE OSPOL

Function: To compute the atmospheric intrinsic reflectance for the case of either satellite or aircraft observation. Also, to compute the downward radiation field needed for the integral formula of $\bar{\rho}$ and $\bar{\rho}'$ (see Chapter I, §2.5.1, Eqs. (25)-(26)) used in the computation in case of a non-Lambertian target.

Description: The general purpose of the successive order of scattering is to solve numerically the equation of radiative transfer for upward (Eq. (1)) and downward radiation (Eq. (2)) for any optical thickness τ . If τ_1 is the total optical thickness and μ the cosine of the view angle, then we can write:

$$I(\tau; \mu, \phi) = I(\tau_1; \mu, \phi) e^{-(\tau_1 - \tau)/\mu} + \int_{\tau}^{\tau_1} J(\tau'; \mu, \phi) e^{-(\tau' - \tau)/\mu} \frac{d\tau'}{\mu} \quad (1 \geq \mu \geq 0) \quad (1)$$

$$I(\tau; -\mu, \phi) = I(0; -\mu, \phi) e^{-\tau/\mu} + \int_0^{\tau} J(\tau'; -\mu, \phi) e^{-(\tau' - \tau)/\mu} \frac{d\tau'}{\mu} \quad (1 \geq \mu \geq 0) \quad (2)$$

where the source function $I(\tau; \mu, \phi)$ accounts for the interaction of the present radiation field with the particles of a layer located at τ , so that:

$$J(\tau; \mu, \phi) = \frac{\omega_0}{4\pi} \int_0^{2\pi} \int_{-1}^1 I(\tau; \mu', \phi') P(\mu, \phi; \mu', \phi') d\mu' d\phi' + \frac{\omega_0}{4\pi} \pi F_0 P(\mu, \phi; -\mu_0, \phi_0) e^{-\tau/\mu_0} \quad (3)$$

The second term of Eq. (3) represents the sun source F_0 transversing the path along (μ_0, ϕ_0) directly to the level τ and then being scattered in direction (μ, ϕ) (primary scattering).

To solve this differential equation, one has to fix boundary conditions which are:

$$I(0; -\mu, \phi) = 0 \quad (4)$$

$$I(\tau_1; \mu, \phi) = 0 \quad (5)$$

These conditions express the fact that there is neither diffuse downward nor upward radiation at the top and bottom of a finite atmosphere.

The convention is to describe the atmosphere with the top at $\tau=0$ and the bottom at $\tau=\tau_1$. The upward radiation correspond to $+\mu$ and the downward to $-\mu$ with $(1 \geq \mu > 0)$, as depicted in Fig. 1.

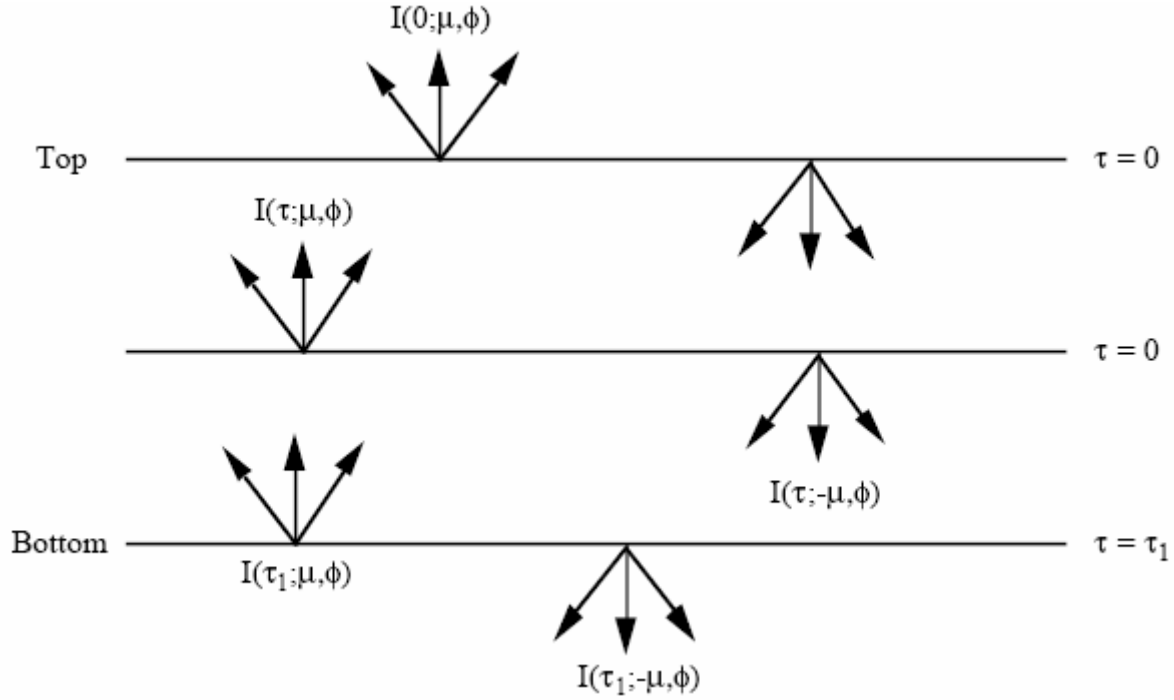


Fig. 1. Schematic view of the radiative transfer problem for a plane parallel atmosphere.

Within the successive order of scattering method, the equation of radiative transfer is solved numerically by iteration. First, the equation is solved for each layer considering only the primary scattering radiation (one interaction between the source (sun) and the atmosphere), giving for Eqs. (1) and (2):

$$I^{(1)}(\tau; \mu, \phi) = \frac{\omega_0}{4\pi} \pi F_0 P(\mu, \phi; -\mu_0, \phi_0) e^{-\tau/\mu_0} \quad (1 \geq \mu \geq 0) \quad (6)$$

$$I^{(1)}(\tau; -\mu, \phi) = \frac{\omega_0}{4\pi} \pi F_0 P(-\mu, \phi; -\mu_0, \phi_0) e^{-\tau/\mu_0} \quad (1 \geq \mu \geq 0) \quad (7)$$

Then for higher orders of scattering we write

$$I^{(n)}(\tau_j; \mu, \phi) = \frac{1}{\mu} \sum_{i=j}^p J^{(n)}(\tau_i; \mu, \phi) e^{-[\tau_j - \tau_i]/\mu} \Delta\tau \quad (8)$$

$$I^{(n)}(\tau_j; -\mu, \phi) = \frac{1}{\mu} \sum_{i=j}^j J^{(n)}(\tau_i; -\mu, \phi) e^{-[\tau - \tau_i]/\mu} \Delta\tau \quad (9)$$

where p represents the number of layers used for the decomposition of the atmosphere, τ_j the optical thickness at level j and $\Delta\tau$ is the increment in optical thickness between two successive layers. $J^{(n)}$ is computed from $I^{(n-1)}$ as:

$$J^{(n)}(\tau; \mu, \phi) = \frac{\Omega_0}{4\pi} \int_0^1 \int_{-1}^{2\pi} I^{(n)}(\tau; \mu', \phi') P(\mu, \phi; \mu', \phi') d\mu' d\phi' \quad (10)$$

Within the code, a numerical integration of Eq. (10) is performed using the decomposition in Fourier series (for ϕ), Legendre polynomials (for the phase function) and Gaussian quadrature (for μ).

The effects of polarization are included through the calculation of four components of the Stokes vector, $\vec{I} = \{I, Q, U, V\}$. The first component, I , describes the intensity of radiation; the other three characterize perpendicular (Q), parallel (U) and elliptical (V) polarization. The degree, angle and ellipticity of polarization are easily calculated from these last three components using simple mathematical formulas. Under the assumption of linearly polarized light, which is the case of 6SV1, $V = 0$. In scalar mode, $\vec{I} = \{I, 0, 0, 0\}$.

References:

- K.-N. Liou, An introduction to atmospheric radiation (Academic Press, Inc., California, 1980).
- J. E. Hansen and L. D. Travis, Light scattering in planetary atmospheres, *Space Science Reviews*, 16, 527-610, 1974.
- J.L. Deuzé, M. Herman, and R. Santer, Fourier series expansion of the transfer equation in the atmosphere-ocean system, *Journal of Quantitative Spectroscopy and Radiative Transfer*, 41(6), 483-494, 1989.
- J. W. Hovenier, C. van der Mee, and H. Domke, Transfer of polarized light in planetary atmospheres: basic concepts and practical methods (Kluwer Academic Publishers, Dordrecht, the Netherlands, 2004).

SUBROUTINE SCATRA

Function: To compute the scattering transmission functions for three atmospheric models: Rayleigh, aerosol and a mixture of both along two paths (downward and upward). Also, to compute the spherical albedo.

Description: As in ATMREF, we have to compute the transmission function and albedo for three different atmospheres and three sensor configurations. The successive order of scattering method (subroutine ISO) is used for the aerosol and mixed cases, or when the sensor is inside the atmosphere on board an aircraft. In case of a Rayleigh atmosphere, we use an accurate analytical formula which has sufficient accuracy and enables us to save computer time. The formula is explicitly coded into SCATRA for the transmission; and CSALBR is called for the albedo. For ground measurements, the upward transmission is set to 1.0 and the spherical albedo to 0.0, because we neglect the atmosphere between the sensor and the target.

We only give here the formula of the Rayleigh transmission, which is based on the two stream method adapted to the case of a single scattering albedo equal to 1.0 (Rayleigh case). The total transmission $T(\mu)$ on the path of length μ can be approximated by:

$$T(\mu) = \frac{[(2/3) + \mu] + [(2/3) - \mu] e^{-\frac{\tau^R}{\mu}}}{(4/3) + \tau^R} \quad (1)$$

where τ^R is the Rayleigh optical thickness and μ is the cosine of the solar/observation angle. The accuracy of Eq. (1) versus the "exact" computation (successive orders of scattering) is illustrated in Fig.1.

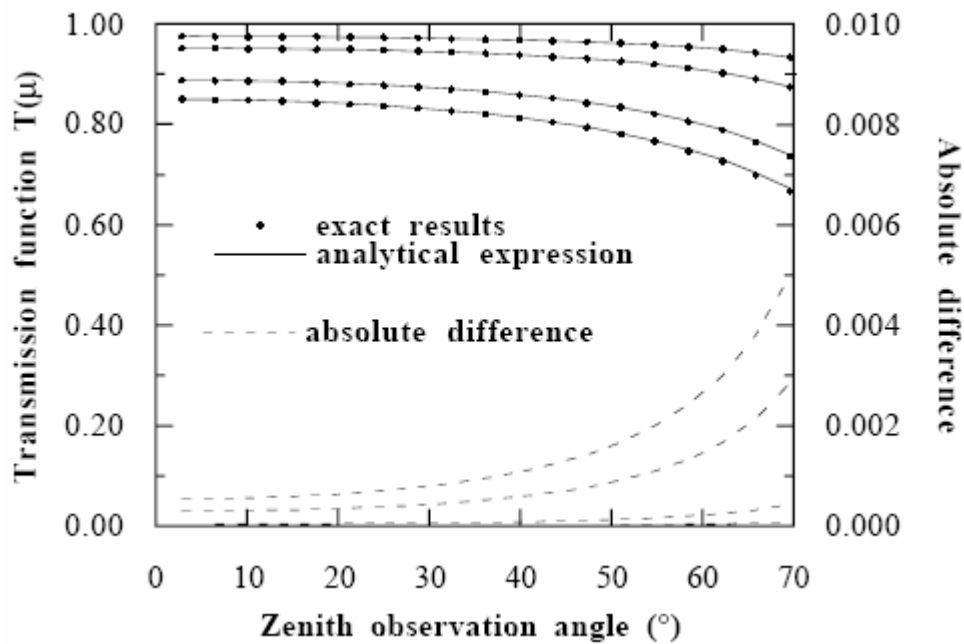


Fig. 1. Accuracy of Eq. (1).

References:

- J.H. Joseph, W.J. Wiscombe, and J.A. Weinman, The Delta-Eddington approximation for radiative flux transfer, *Journal of the Atmospheric Sciences*, 33, 2242-2459, 1976.
- W.E. Meador and W.R. Weaver, Two-Stream approximations to radiative transfer in planetary atmospheres: a unified description of existing methods and a new improvement, *Journal of the Atmospheric Sciences*, 37, 630-643, 1980.
- R.H. Welch and W.G. Zdunkowski, Back scattering approximations and their influence on Eddington-Type solar flux calculation, *Beitraege zur Physik der Atmosphaere*, 55(1), 28-42, 1982.
- W.G. Zdunkowski, R.M. Welch, and G. Korb, An investigation of the structure of typical two-stream methods for the calculation of solar fluxes and heating rates in clouds, *Beitraege zur Physik der Atmosphaere*, 53(2), 147-166, 1980.

SUBROUTINE TRUNCA

Function: To decompose the aerosol phase function in a series of Legendre polynomials used in the OSPOL and ISO subroutines.

Reference:

J. Lenoble, Radiative Transfer in scattering and absorbing atmospheres: standard computational procedures, 83-84, A. Deepak Publishing, 1985.